

REPORT DOCUMENTATION PAGE			Form Approved OMB NO. 0704-0188		
<p>The public reporting burden for this collection of information is estimated to average 1 hour per response, including the time for reviewing instructions, searching existing data sources, gathering and maintaining the data needed, and completing and reviewing the collection of information. Send comments regarding this burden estimate or any other aspect of this collection of information, including suggestions for reducing this burden, to Washington Headquarters Services, Directorate for Information Operations and Reports, 1215 Jefferson Davis Highway, Suite 1204, Arlington VA, 22202-4302. Respondents should be aware that notwithstanding any other provision of law, no person shall be subject to any penalty for failing to comply with a collection of information if it does not display a currently valid OMB control number. PLEASE DO NOT RETURN YOUR FORM TO THE ABOVE ADDRESS.</p>					
1. REPORT DATE (DD-MM-YYYY)		2. REPORT TYPE New Reprint		3. DATES COVERED (From - To) -	
4. TITLE AND SUBTITLE Bionanomaterials and Bioinspired Nanostructures for Selective Vapor Sensing			5a. CONTRACT NUMBER		
			5b. GRANT NUMBER W911NF-10-C-0069		
			5c. PROGRAM ELEMENT NUMBER 0D10BD		
6. AUTHORS Radislav Potyrailo, Rajesh R. Naik			5d. PROJECT NUMBER		
			5e. TASK NUMBER		
			5f. WORK UNIT NUMBER		
7. PERFORMING ORGANIZATION NAMES AND ADDRESSES GE Global Research One Research Circle Niskayuna, NY 12309 -1027			8. PERFORMING ORGANIZATION REPORT NUMBER		
9. SPONSORING/MONITORING AGENCY NAME(S) AND ADDRESS (ES) U.S. Army Research Office P.O. Box 12211 Research Triangle Park, NC 27709-2211			10. SPONSOR/MONITOR'S ACRONYM(S) ARO		
			11. SPONSOR/MONITOR'S REPORT NUMBER(S) 58113-CH-DRP.3		
12. DISTRIBUTION AVAILABILITY STATEMENT Approved for public release; distribution is unlimited.					
13. SUPPLEMENTARY NOTES The views, opinions and/or findings contained in this report are those of the author(s) and should not be construed as an official Department of the Army position, policy or decision, unless so designated by other documentation.					
14. ABSTRACT At present, monitoring of air at the workplace, in urban environments, and on battlefields; exhaled air from medical patients; air in packaged food containers; and so forth can be accomplished with different types of analytical instruments. Vapor sensors have their niche in these measurements when an unobtrusive, low-power, and cost-sensitive technical solution is required. Unfortunately, existing vapor sensors often degrade their vapor quantitation					
15. SUBJECT TERMS vapor sensors, bionanomaterials, bioinspired nanostructures					
16. SECURITY CLASSIFICATION OF:		17. LIMITATION OF ABSTRACT		15. NUMBER OF PAGES	19a. NAME OF RESPONSIBLE PERSON
a. REPORT UU	b. ABSTRACT UU	c. THIS PAGE UU	UU		Radislav Potyrailo
				19b. TELEPHONE NUMBER 518-387-7870	

Report Title

Bionanomaterials and Bioinspired Nanostructures for Selective Vapor Sensing

ABSTRACT

At present, monitoring of air at the workplace, in urban environments, and on battlefields; exhaled air from medical patients; air in packaged food containers; and so forth can be accomplished with different types of analytical instruments. Vapor sensors have their niche in these measurements when an unobtrusive, low-power, and cost-sensitive technical solution is required. Unfortunately, existing vapor sensors often degrade their vapor-quantitation accuracy in the presence of high levels of interferences and cannot quantitate several components in complex gas mixtures. Thus, new sensing approaches with improved sensor selectivity are required. This technological task can be accomplished by the careful design of sensing materials with new performance properties and by coupling these materials with the suitable physical transducers. This review is focused on the assessment of the capabilities of bionanomaterials and bioinspired nanostructures for selective vapor sensing. We demonstrate that these sensing materials can operate with diverse transducers based on electrical, mechanical, and optical readout principles and can provide vapor-response selectivity previously unattainable by using other sensing materials. This ability for selective vapor sensing provides opportunities to significantly impact the major directions in development and application scenarios of vapor sensors.

REPORT DOCUMENTATION PAGE (SF298)
(Continuation Sheet)

Continuation for Block 13

ARO Report Number 58113.3-CH-DRP
Bionanomaterials and Bioinspired Nanostructure..

Block 13: Supplementary Note

© 2013 . Published in Annual Review of Materials Research, Vol. Ed. 0 43, (1) (2013), (, (1). DoD Components reserve a royalty-free, nonexclusive and irrevocable right to reproduce, publish, or otherwise use the work for Federal purposes, and to authorize others to do so (DODGARS §32.36). The views, opinions and/or findings contained in this report are those of the author(s) and should not be construed as an official Department of the Army position, policy or decision, unless so designated by other documentation.

Approved for public release; distribution is unlimited.

Bionanomaterials and Bioinspired Nanostructures for Selective Vapor Sensing

Radislav Potyrailo¹ and Rajesh R. Naik²

¹Chemistry and Chemical Engineering, General Electric Global Research Center, Niskayuna, New York 12309; email: potyrailo@crd.ge.com

²Materials and Manufacturing Directorate, Air Force Research Laboratory, Wright-Patterson Air Force Base, Ohio 45433

Annu. Rev. Mater. Res. 2013. 43:307–34

First published online as a Review in Advance on April 3, 2013

The *Annual Review of Materials Research* is online at matsci.annualreviews.org

This article's doi:
10.1146/annurev-matsci-071312-121710

Copyright © 2013 by Annual Reviews.
All rights reserved

Keywords

vapor sensors, bionanomaterials, bioinspired nanostructures, multivariable individual sensors, wireless sensing, battery-independent sensor operation, distributed sensor networks, unobtrusive sensors

Abstract

At present, monitoring of air at the workplace, in urban environments, and on battlefields; exhaled air from medical patients; air in packaged food containers; and so forth can be accomplished with different types of analytical instruments. Vapor sensors have their niche in these measurements when an unobtrusive, low-power, and cost-sensitive technical solution is required. Unfortunately, existing vapor sensors often degrade their vapor-quantitation accuracy in the presence of high levels of interferences and cannot quantitate several components in complex gas mixtures. Thus, new sensing approaches with improved sensor selectivity are required. This technological task can be accomplished by the careful design of sensing materials with new performance properties and by coupling these materials with the suitable physical transducers. This review is focused on the assessment of the capabilities of bionanomaterials and bioinspired nanostructures for selective vapor sensing. We demonstrate that these sensing materials can operate with diverse transducers based on electrical, mechanical, and optical readout principles and can provide vapor-response selectivity previously unattainable by using other sensing materials. This ability for selective vapor sensing provides opportunities to significantly impact the major directions in development and application scenarios of vapor sensors.

1. INTRODUCTION

Vapor and gas detection is critical for numerous everyday applications ranging from process and environmental monitoring to home, industrial, and homeland safety and security. For these and other applications, there are several types of analyzers based on different technologies, including gas chromatography, mass spectrometry, ion mobility spectrometry, and sensors. Vapor sensors are analytical devices in which a sensing material either is applied onto a suitable physical transducer or simultaneously also serves as a transducer to convert a change in a property of a sensing material into a readable form of energy (1, 2). The obtained signal from the transducer provides useful information about the concentration of species in the sample. The operational advantages of vapor sensors over other field-portable analytical instruments include (a) continuous real-time determination of the concentrations of specific sample constituents, (b) low power consumption, (c) operation without consumables, and (d) unobtrusive form factors.

Response of vapor sensors should be considered on several levels ranging from response to almost all gases and vapors, to response to only a specific vapor, and finally to response to the vapor of interest in the presence of gaseous interferences and uncontrolled operating conditions (see **Figure 1**). Most materials demonstrated for sensing are sensitive not only to target analytes, but also to a wide variety of vapors (see **Figure 1a**). The presence of gaseous interferences complicates sensor measurements (see **Figure 1b**), significantly degrading the accuracy of sensor performance. Variable or uncontrolled operating conditions, e.g., temperature fluctuations (see **Figure 1c**), further reduce the sensor accuracy.

Although the design of a sensor for a particular application is dictated by the nature and requirements of its application, it is useful to define the features that one would wish of an ideal vapor sensor. These features include high accuracy, high precision, broad dynamic range, high sensitivity, high selectivity, long-term stability, maintenance simplicity, fast response speed, low initial cost, low operation cost, response reversibility, small size, low power consumption, robustness, self-calibration, and others (1). The qualities of an ideal sensor are often weighted differently according to a particular application. For numerous applications, sensitivity, selectivity, and response speed are among the most important requirements (3, 4). Significant improvement in the

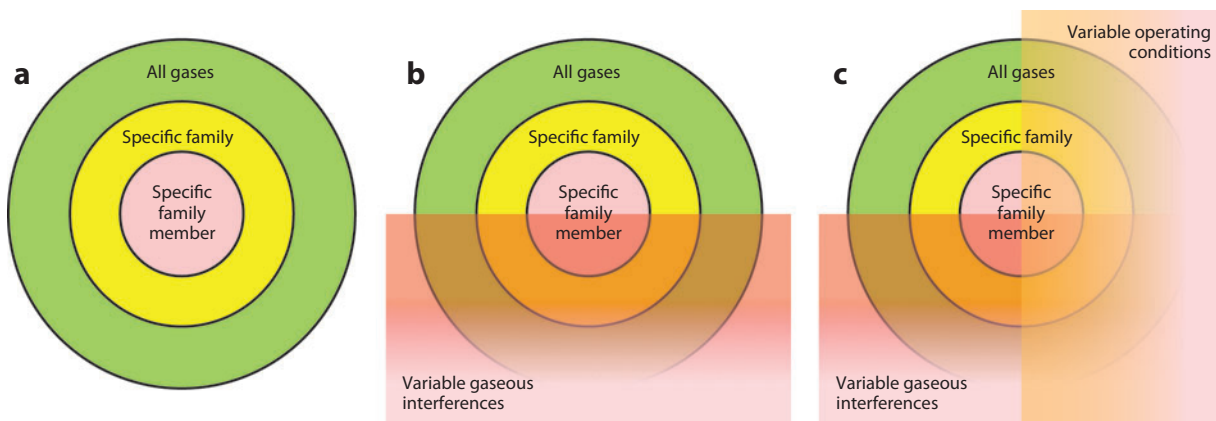


Figure 1

Levels of needed performance of sensor systems. (a) A sensor is sensitive to all vapors (a completely nonselective sensor), to only a specific family of vapors (a partially selective sensor), or to a specific family member of vapors (a fully selective sensor). (b) The presence of gaseous interferences complicates sensor measurements by degrading the accuracy of sensor performance. (c) Variable or uncontrolled operating conditions (e.g., temperature fluctuations) further reduce the accuracy of sensor performance.

sensitivity of sensors has been demonstrated by using new sensing materials, transducer designs, and operation in vacuum or in dry carrier gas (5–7). High-surface-area sensing materials significantly increase the response speed (8). However, high selectivity remains the most significant challenge for existing sensors and has yet to be achieved in sensor design (2, 4, 9, 10). Existing vapor sensors often cannot perform highly selective vapor detection in the presence of high levels of interferences, cannot quantitate several components in gas mixtures, and cannot provide accurate vapor determinations in the presence of uncontrolled fluctuations of ambient temperature. These practical scenarios are often probable in numerous applications. Examples of present and upcoming demanding applications for sensors in complex environments include monitoring air at the workplace, in urban environments, and on battlefields; monitoring exhaled air from medical patients; monitoring air in packaged food containers; and detecting diseased agricultural crops. To meet the requirements for these and other demanding applications, new sensing approaches with improved sensor selectivity are required. This technological task can be accomplished by the careful design of sensing materials with new performance properties and by coupling these materials with the suitable physical transducers.

This review is focused on assessing the capabilities of bionanomaterials and bioinspired nanostructures for selective vapor sensing. We demonstrate that these sensing materials can operate with diverse transducers based on electrical, mechanical, and optical readout principles and can provide vapor-response selectivity previously unavailable from other sensing materials. The vapor-response selectivity of these materials is attractive for their implementation in numerous practical applications. Bionanomaterials have been explored for vapor sensing in the form of biomolecule-based sensing films and for functionalization of diverse nanomaterials such as carbon nanotubes (CNTs), graphene, semiconducting inorganic nanowires, semiconducting conjugated polymer nanotubes, and metal nanoparticles. Vapor sensing with bioinspired nanostructures also brings important vapor-response selectivity when coupled with multivariable optical transducers. These nanophotonic sensors are based on vapor responses of biological structures with future nanofabricated biomimetic designs and with bioinspired, structurally colored, colloidal crystal films. This ability for selective vapor sensing provides opportunities to significantly impact the major directions in development and application scenarios of vapor sensors.

2. TRANSDUCER TECHNOLOGIES

2.1. Transducer Types

The energy-transduction principles that are employed for chemical sensing involve radiant, mechanical, electrical, and thermal types of energy (11). Transducers based on the radiant type of energy utilize design principles based on intensity, frequency, phase, polarization, and time-domain detection methods of sensing material response and their associated transducer designs. Transducers based on the mechanical type of energy utilize design principles based on measurements of mass and viscoelastic responses of sensing materials. Examples of such transducers include cantilevers and numerous types of acoustic resonators ranging from tuning forks to thickness shear mode (TSM) resonators also known as quartz crystal microbalances (QCMs) to surface acoustic wave (SAW) resonators, bulk acoustic wave (BAW) resonators, and other devices. Transducers based on the electrical type of energy utilize different design principles to measure resistance, current, capacitance, impedance, work function, and some other electrical properties related to the electrical responses of sensing materials. Examples of such transducers include nonresonant transducers such as chemiresistors, chemicapacitors, and field effect transistors (FETs) and resonant transducers such as inductor-capacitor-resistor (LCR) resonators. Also, TSM, SAW, and other

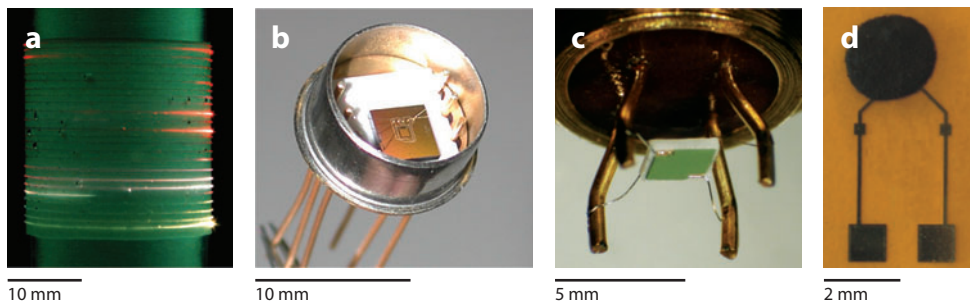


Figure 2

Examples of transducers that are based on different energy-transduction principles and that have been employed for chemical sensing. (a) An example of radiant energy transduction is an intensity-based distributed fiber-optic sensor with its siloxane cladding chemically modified with an absorbing dye (shown in the photo as scattering red light; in contrast, unmodified cladding scatters white light). (b) An example of mechanical energy transduction is a micromachined cantilever with a deposited polycarbonate as a sensing material. Adapted with permission from Reference 12. (c) An example of electrical energy transduction is a resistor with a deposited metal oxide semiconducting sensing material on one side and a microheater on the other side of the substrate. (d) An example of thermal energy transduction is a resistor formed on a flexible polyimide foil, passivated by a layer of photo resist, and catalytically activated by MnO_2 . Adapted with permission from Reference 13.

acoustic resonators can be utilized for measurements of electrical properties of sensing materials. Transducers based on the thermal type of energy utilize different design principles to measure calorimetric response of sensing materials. **Figure 2** shows representative examples of transducers that are based on different energy-transduction principles and that have been employed for chemical sensing.

2.2. Sensor Arrays

The requirement for sensor selectivity often conflicts with the requirement for sensor reversibility because the full reversibility of sensor response is achieved via weak interactions between the analyte and the sensing film, whereas the high selectivity of sensor response is achieved via strong interactions between the analyte vapor and the sensing film. As a result, the fundamental nature of adsorption and absorption interactions between vapors and materials typically does not provide high molecular-recognition selectivity compared with that in biomolecular interactions (2, 8).

Table 1 summarizes the vapor-response mechanisms of some of the most widely studied types of sensing materials (6, 9, 14–25). Despite the significant diversity of mechanisms, no fully selective vapor-sensing materials are yet available. As an example, **Figure 3** illustrates typical response cross-sensitivity for different types of sensing materials toward a variety of vapors (23, 24, 26–31). A common approach to address the problem of poor selectivity of individual sensors is to build an array of partially selective sensors (32) and to process the array response by using multivariate analysis (33). In such sensor arrays, individual transducers are coated with sensing materials, and the response of the sensing material (e.g., resistance, current, capacitance, work function, mass, temperature, optical thickness, light intensity) is measured. The use of multitransducer sensor arrays based on different detection principles provides a way to further enhance response selectivity (10). Examples include cantilever-capacitor-calorimeter (34), resistor-TSM (35), capacitor-TSM (36), and resistor-SAW (37) arrays. **Figure 4** illustrates examples of some sensor arrays with different numbers of sensors and different transducers in an array (34, 38–42).

Table 1 Response mechanisms of different sensing materials for gases and vapors (6, 9, 14–25)

Type of sensing material	Response mechanisms	Reference(s)
Dielectric polymers	Dispersion, polarizability, dipolarity, basicity, acidity, and hydrogen bonding interactions	9
Conjugated polymers	Changes in density and charge carrier mobility, swelling, and conformation transitions of chains	14, 15
Metal porphyrins, phthalocyanines, and related macrocycles	Hydrogen bonding, polarization, polarity, metal center coordination interactions, π stacking, and molecular arrangements	16, 17
Cavitanids	Intracavity host-guest complexation with hydrogen bonding, CH- π , and dipole-dipole as the main specific interactions	18
Zeolites	Molecular discrimination by size, shape, molecular kinetic diameter	19
Metal-organic frameworks	van der Waals interactions of the framework surface, coordination to the central metal ion, hydrogen bonding of the framework surface, size exclusion	20, 21
Monolayer-protected metal nanoparticles	Sorption of vapors in insulating regions, electron tunneling between metal cores, charge hopping along the atoms of ligand shell	22, 23
Carbon nanotubes	Charge transfer from analytes and polarization of surface adsorbates, gas-induced Schottky barrier modulation	24, 25
Graphene	Charge transfer induced by adsorption/desorption of gaseous molecules acting as electron donors or acceptors, leading to changes in conductance	6

When a sensor array response is processed by using multivariate analysis tools, the goal is to provide qualitative analysis by extracting response patterns and identifying types of detected analytes or to provide quantitative analysis of concentrations of one or several analytes (33, 43). The most widely implemented pattern-recognition technique for multivariate signals is principal-components analysis (PCA) (33). **Figure 5** summarizes the principle of data processing using PCA and the main aspects of the PCA-based pattern recognition. PCA is a robust, unsupervised technique that reduces the data dimensionality by presenting the data as the weighted sums [principal components (PCs)] of the original inputs from each sensor.

2.3. Multivariable Individual Sensors

Multivariable sensors are devices that provide several partially or fully independent responses from an individual sensor. The key for such multivariable response of an individual sensor is a proper combination of a multivariable transducer with a sensing material. Different approaches have been reported for building multivariable sensors. Simultaneous measurements of capacitance and resistance of CNT sensing materials were performed, demonstrating the ability to discriminate between different vapors on the basis of their different ratios of capacitance and resistance responses (44). Multiparameter vapor sensing was also demonstrated by using FETs (45) and temperature-programmed sensors (46). Impedance spectroscopy measurements were performed on TSM (47) and interdigital (48) sensors to extract several independent parameters. Also measured were independent output parameters of individual acoustic wave transducers, for example, wave propagation velocity and attenuation (49), series-resonant frequency and resonant admittance (50), and material resistance and resonance frequency (51). Researchers described sensors based on dissipation spectroscopy that measured the magnitudes of the high-frequency conductivity changes in semiconducting sensing films related to different vapors (52, 53). Low-frequency noise spectra have also been utilized to distinguish between different vapors (54).

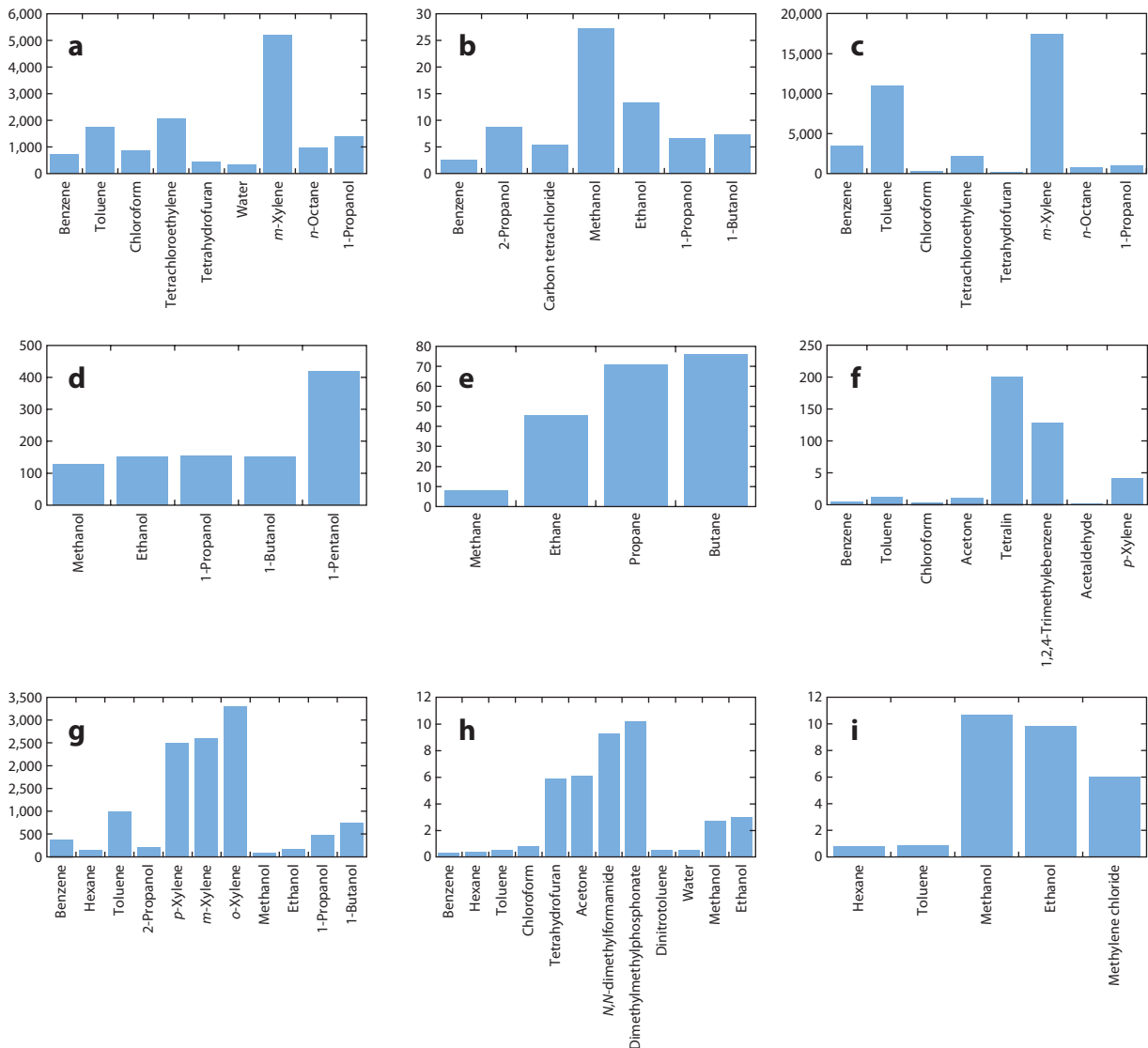


Figure 3

Typical vapor-response selectivity of different types of sensing materials. (a) Dielectric polymers. The vapor partition coefficient K of polyetherurethane is determined by using thickness shear mode (TSM) sensors. From Reference 26. (b) Conjugated polymers. Shown is the resistance response $\Delta R/R$ (%) of polypyrrole doped with camphorsulfonic acid upon exposure to saturated vapors. From Reference 27. (c) Metal phthalocyanines. Shown is the vapor partition coefficient K of nickel phthalocyanine by using TSM sensors. From Reference 26. (d) Cavitands. The frequency shift ΔF of phosphorus-bridged cavitand upon exposure to 3,000 ppm of vapors is measured by using TSM sensors. From Reference 28. (e) Zeolites. Potentiometric vapor response ΔU of Pt-loaded zeolite Na-ZSM-5 upon exposure to 1,000 ppm of vapors. From Reference 29. (f) Metal-organic frameworks. Henry's constant K_H in IRMOF-1. From Reference 30. (g) Monolayer-protected metal nanoparticles. Vapor partition coefficient K of octanethiol-Au nanoparticles determined by using TSM sensors. From Reference 23. (h) Carbon nanotubes. Shown is the capacitance response $(\Delta C/C) \times 10^{-3}$ of bare single-walled carbon nanotubes upon exposure to 0.01 P/P_0 of vapors. From Reference 24. (i) Graphene. Shown is the resistance response $\Delta R/R$ (%) of reduced graphene oxide upon exposure to saturated vapors. From Reference 31. The y axes in panels $a-i$ represent the corresponding sensor responses.

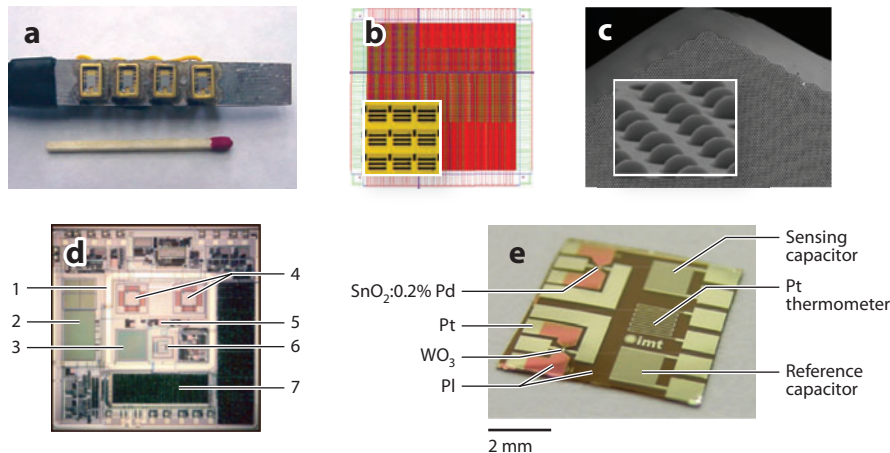


Figure 4

Examples of sensor arrays with different numbers of sensors and different types of transducers in an array. (a) An array of four thickness shear mode sensors for operation with polymeric sensing films. (b) An array of 4,096 interdigital electrode resistor sensors for operation with conjugated polymeric sensing films with the capability for operation with 65,536 sensors. The size of the die is 2.1 cm × 2.1 cm. The inset shows nine individual interdigital electrode resistors. Adapted with permission from Reference 39. (c) Portion of an imaging fiber-optic bundle sensor array that contains thousands of microwells etched into one face of an imaging fiber-optic bundle and filled with diverse dye-doped microspheres. The inset shows microbead sensors in etched microwells. Each individual fiber core is 4.5 μm. Adapted with permission from Reference 41. (d) A multitransducer vapor microsensor system chip (7 × 7 mm size) with different components that include (1) a flip-chip frame, (2) a reference capacitor, (3) a sensing capacitor, (4) a calorimetric sensor and reference, (5) a temperature sensor, (6) a mass-sensitive resonant cantilever and (7) a digital interface. Adapted with permission from Reference 34. (e) A multitransducer vapor microsensor system on polyimide (PI) foil with two metal oxide and two capacitive gas sensors and a resistive thermometer. Adapted with permission from Reference 42.

A powerful approach for building multivariable transducers was recently developed by using a variety of resonant devices. Several examples of the resulting multivariable sensors are illustrated in **Figure 6** and utilize acoustic wave (**Figure 6a,b**) and LCR (**Figure 6c,d**) transducers (55–58) coupled with sensing materials that exhibit different response mechanisms for different species of interest. For selective analyte quantitation using individual sensors, impedance spectra of the resonator were measured, and several parameters from the measured real $Z_{re}(f)$ and imaginary $Z_{im}(f)$ portions of the impedance spectra were further calculated. These parameters included frequency position F_p and magnitude Z_p of $Z_{re}(f)$, resonant F_1 and antiresonant F_2 frequencies, and their respective magnitudes Z_1 and Z_2 of $Z_{im}(f)$ (57, 58). By applying multivariate analysis to the impedance spectra or to the calculated parameters, quantitation of analytes and their mixtures with interferences was performed with individual sensors (59, 60).

Importantly, this approach for the improvement of sensor performance is very general. The implemented transducers include TSM (**Figure 6a**) and SAW (**Figure 6b**) devices as well as LCR resonators operating in different frequency ranges such as the radiofrequency (kilohertz to megahertz) range (**Figure 6c**) and the microwave (gigahertz) range; an LCR resonator can be a split-ring resonator (SRR) or a dual SRR (**Figure 6d**) (4, 61, 62). Operation of the LCR circuits at higher frequencies is also possible, leading to transducers operating in the optical spectral range.

Importantly, these developed LCR sensors operate not only with semiconducting materials to achieve the desired response selectivity via changes in the conductivity and capacitance of

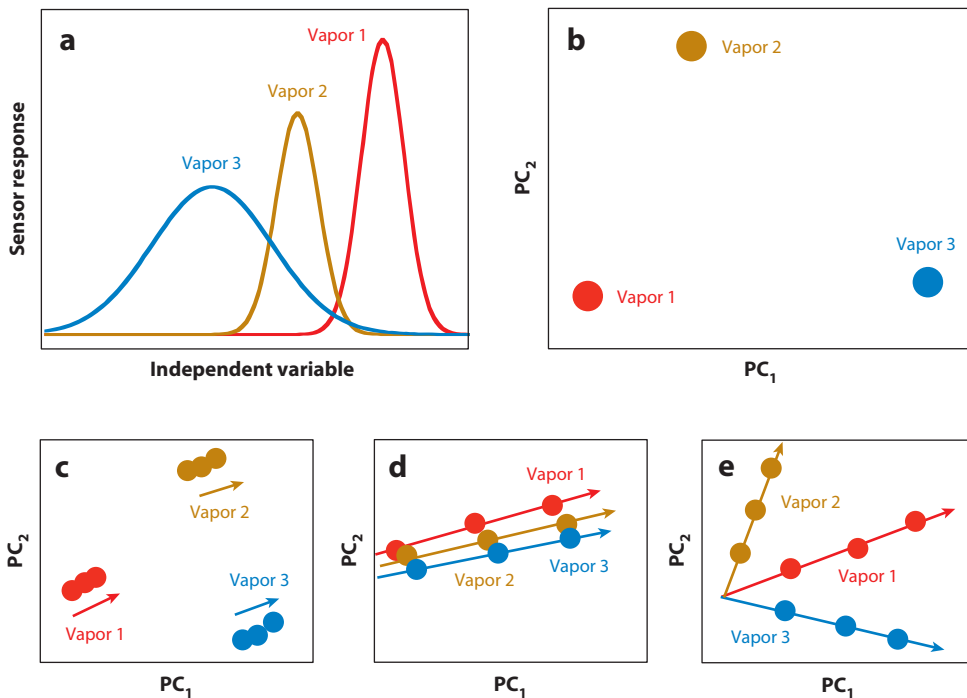


Figure 5

The principle of data processing using principal-components analysis (PCA) and the main aspects of PCA-based pattern recognition. (a) Three simulated Gaussian curves with variable height and width for PCA exemplary processing. (b) A scores plot of a PCA model based on the data from the three simulated Gaussian curves. (c–e) Three general scenarios of PCA scores plots: (c) poor sensitivity and good selectivity, (d) good sensitivity and poor selectivity, and (e) good sensitivity and good selectivity. PC₁, PC₂, and PC₃ denote principal components 1, 2, and 3, respectively.

semiconducting sensing films (44, 52, 63), but also with dielectric polymers (4, 59). One of these polymers, polyetherurethane (PEUT), was used to demonstrate selective detection of individual vapors with a single sensor (**Figure 7**). Sensor response depended on the dielectric constants ϵ_r of the measured vapors as well as on ϵ_r of the sensing film; the net capacitance either increased or decreased upon vapor exposure. For PEUT sensing films ($\epsilon_r = 4.8$), the sensor capacitance increased upon exposure to vapors with the dielectric constants higher than the sensing film [e.g., tetrahydrofuran (THF) ($\epsilon_r = 7.5$), ethyl acetate ($\epsilon_r = 6.0$), and propanol ($\epsilon_r = 20.1$)], and decreased upon exposure to vapors of lower dielectric constant [e.g., benzene ($\epsilon_r = 2.3$)]. The individual F_p , F_1 , F_2 , Z_p , Z_1 , and Z_2 responses (**Figure 7a,b**) were analyzed by using PCA tools, and the results are shown in **Figure 7c**. This single sensor with a multivariable response was able to easily discriminate between benzene and propanol but was unable to discriminate between tetrahydrofuran and ethyl acetate at these relatively low concentrations P/P_0 , where P is vapor partial pressure and P_0 is the saturated vapor pressure.

Another recently demonstrated general design of the multivariable sensors was based on bio-inspired approaches and utilized dielectric resonators (**Figure 8**). One sensor concept was based on the opal-like iridescence of self-assembled photonic crystals (**Figure 8a,b**) (64). Another sensor concept was based on the iridescence of scales of *Morpho* butterflies (**Figure 8c,d**) (65). The reflectance spectra of the self-assembled photonic crystals and the butterfly scales provided

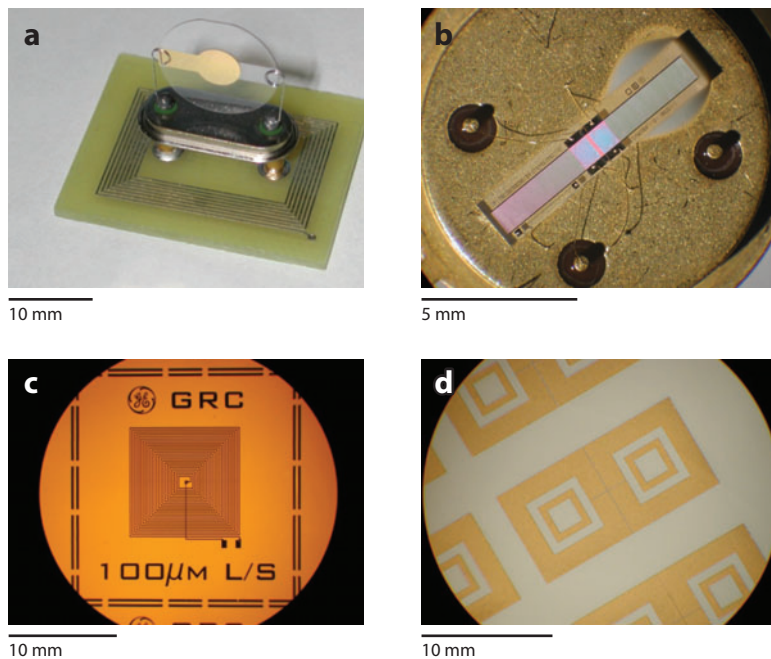


Figure 6

Selected examples of multivariable vapor sensors based on acoustic wave and inductor-capacitor-resistor (LCR) resonators. (a) A thickness shear mode sensor with an inductively coupled readout. (b) A surface acoustic wave sensor. (c) An LCR sensor operating in the radiofrequency range. (d) A dual split-ring resonator as an LCR sensor operating in the microwave frequency range.

information about the nature and concentration of vapors. Other bioinspired approaches for optical detection of vapors were also reported (66–69) but did not apply multivariable transduction principles.

3. BIONANOMATERIALS

Numerous types of biomolecules and biomolecular assemblies have been demonstrated for biosensing of large and small molecules in the aqueous phase, in which highly selective molecular recognition is facilitated by weak interactions through multivalent and cooperative binding. Examples of such bioreceptors include antibodies (70), enzymes (71), aptamers (72), phages (73), olfactory receptor–derived peptides (74), antimicrobial peptides (75), whole cells (76), cell-derived nanovesicles (77), olfactory receptors (78), odorant-binding proteins (79), olfactory neurons (80), carbohydrates (81), and oligosaccharides (82). While applying bioreceptors for the vapor-phase recognition of small molecules and odorants, one should keep in mind that the nature of molecular interactions between the native biomolecules and analytes in the aqueous phase could be altered in the vapor phase. Initial research on the applications of biological molecules as vapor-phase sensing materials goes back to the 1980s (83). At present, vapor-phase sensing using sequence-specific biomolecules such as oligopeptides (84–86) and nucleic acids (87) as well as antibodies (88), lipids (89–92), and amino acids (93) is attracting the interest of a growing number of researchers. The two broad directions in this research area are the use of biomolecules directly as sensing films on physical transducers and as selective moieties for the functionalization of signal-transducing nanomaterials.

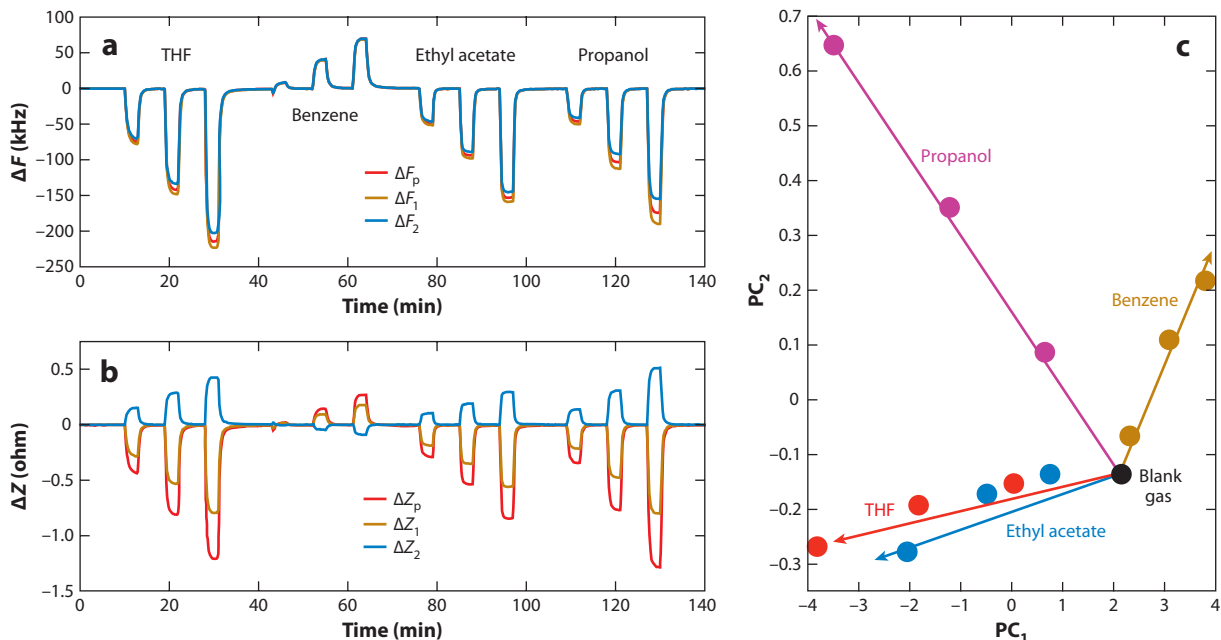


Figure 7

The ability to discriminate between individual vapors [tetrahydrofuran (THF), benzene, ethyl acetate, and propanol] using a multivariable transducer with a dielectric polyetherurethane film. Individual sensor responses (a) F_p , F_1 , F_2 and (b) Z_p , Z_1 , and Z_2 and (c) scores plot of a model of an individual sensor response using principal-components analysis (PCA). Concentrations of vapors are 0, 0.04, 0.07, and 0.11 P/P_0 (THF); 0, 0.09, 0.18, and 0.27 P/P_0 (benzene); and 0, 0.05, 0.11, and 0.16 P/P_0 (ethyl acetate and propanol).

3.1. Biomolecule-Based Films

The rationale for using biomolecules as vapor-sensing films comes from odorant receptor proteins (94) and, in general, from receptors in living cells (95). Different resonant transducers such as TSM (89, 90, 92, 96), SAW (88, 97), and microcantilever resonators (98) were implemented for the detection of vapor responses by using biomolecule-sensing materials. It is possible to compute selective target-binding ability of artificial oligopeptides (84, 85). Thus, artificial oligopeptides were computationally designed to mimic the highly selective aryl hydrocarbon receptor-binding site in living cells (84). The Phe-Gln-Gly backbone of this receptor strongly binds to dioxins and was chosen as the basis for selection of a binding pocket on the basis of amino acid motifs for computational screening of a library of artificial dioxin receptors. Several pentapeptide sequences were computationally identified and synthesized with two terminal cysteine residues. These cysteine residues were used to covalently attach the peptides onto TSM resonators and were able to detect dioxins down to low-parts-per-billion levels. Experimentally determined selectivity against the dioxin vapor correlated well with the calculated binding energy of receptors.

Peptides that resemble binding sites of human olfactory receptor protein have also been identified, synthesized, and tested for their responses to target vapors and interferences (85). From the tertiary structure of olfactory receptors, the odorant-binding domains were expected to be localized on the surface of the transmembrane (TM) domains within an α -helix structure (99). The tertiary structure of the human olfactory receptor protein P30953 was modeled (Figure 9a), followed by computer docking simulations to find binding sites between the model structure and several target vapors, including trimethylamine, ammonia, acetic acid, and *o*-xylene (Figure 9b)

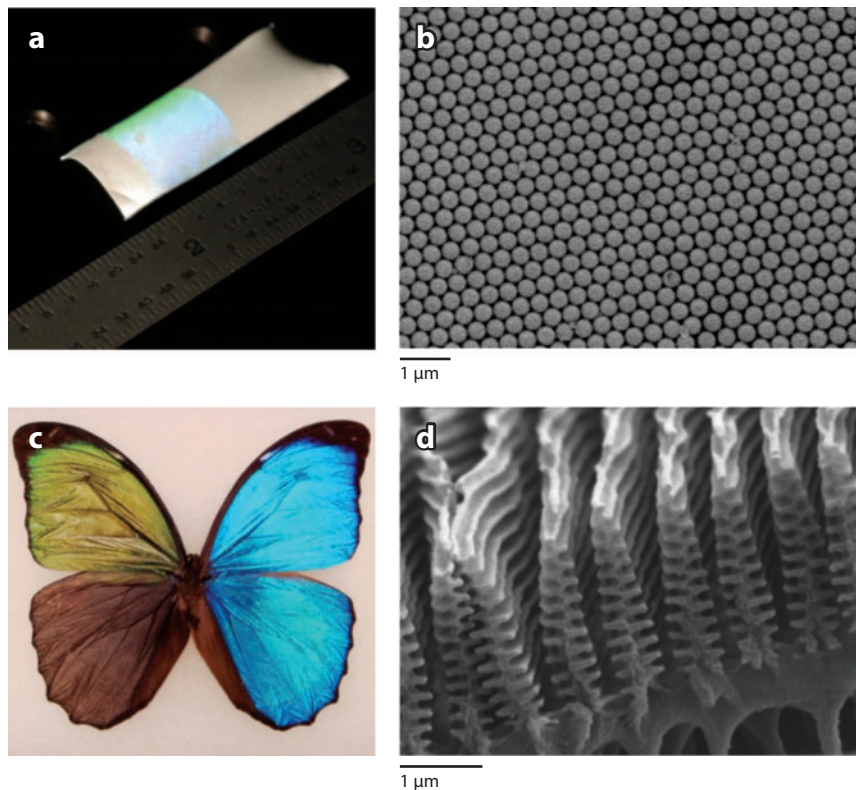


Figure 8

Selected examples of multivariable vapor sensors based on bioinspired dielectric resonators. (a) A photo of a structurally colored composite core/shell colloidal crystal film. (b) Scanning electron microscope (SEM) image of the photonic nanostructure. Panels *a* and *b* are adapted with permission from Reference 64. (c) Photo of an iridescent *Morpho* butterfly demonstrating color changes upon exposure to liquids of different refractive indexes, n . The top left wing was exposed to ethanol solvent ($n = 1.362$), and the bottom left wing was exposed to toluene solvent ($n = 1.497$). (d) An SEM image of the photonic *Morpho* nanostructure.

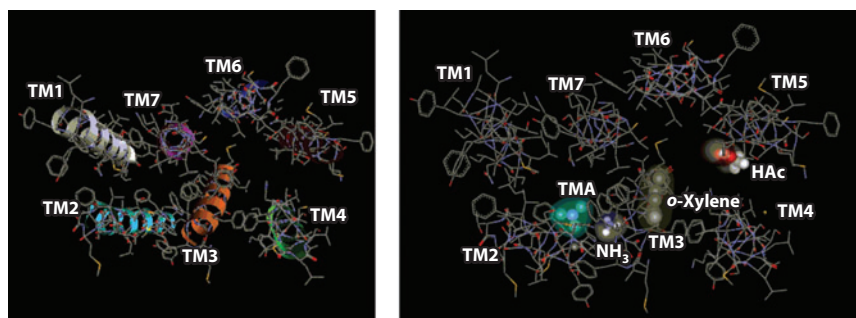


Figure 9

Binding of diverse vapors to the P30953 human olfactory receptor. (a) Molecular model of the tertiary structure of the receptor. (b) Four identified sites responsible for binding of trimethylamine (TMA), ammonia (NH₃), acetic acid (HAc), and *o*-xylene vapors. TM denotes transmembrane. Adapted with permission from Reference 85.

(85). Ligand-binding sequences were identified as those with the most exothermic interactions with the target vapors. Four sites for binding target vapors were located within TM α -helices TM2, TM3, and TM5 (see **Figure 9b**). Polypeptides corresponding to the selective portions of these binding sites were designed, synthesized, and attached to TSM transducers for vapor testing. Each polypeptide demonstrated a strong preferential response to its corresponding vapors with a 3–5-fold-lower response to interferences (85).

Polypeptide sequences with affinity to a wide range of materials were selected by using combinatorial chemistry techniques such as bacterial cell surface and phage-display techniques (100–102). Phage display has been utilized to identify peptides that specifically recognize desired analytes at the molecular level with specific recognition motifs (103). Using mutational analysis, investigators showed that polypeptides with specific recognition motifs can bind trinitrotoluene (TNT) and dinitrotoluene (DNT) vapors through multivalent interactions of these vapors with key side-chain amino acids. DNT-binding peptide receptors were further conjugated to an oligo(ethylene glycol) hydrogel for vapor-phase testing. Experimental results of a vapor-phase binding assay for a DNT-specific film demonstrated a fourfold increase in the partition coefficient for DNT over TNT vapor. Vapor-phase binding performance was attributed to the ability of the oligo(ethylene glycol) hydrogel to maintain the conformation and selectivity of biomolecules. These results demonstrated a successful translation of binding peptide receptors screened in liquid to selective vapor-phase sensing.

Lipid and lipid-like sensing films have also been extensively used for vapor sensing because a wide variety of volatile organic compounds are soluble in lipids (104). This vapor solubility of lipids and lipid-like molecules opens up the possibility to use these molecules for vapor sensing directly attached to a transducer (83, 89), formulated into a polymer matrix (90), formed as mixed-lipid films (91), or grafted with polymers (92).

Deposition of films containing biological molecules for vapor sensing has been explored not only using traditional methods such as immobilization from solution onto transducers (84) and incorporation of biomolecules into hydrogel matrices (103), but also using plasma deposition (96, 105) and molecular effusion (93). Plasma deposition was performed by radio-frequency sputtering to produce films composed of random peptide sequences formed by plasma reactions of individual amino acids during deposition (106). These moderate plasmas were used for the preparation of amino acid films for vapor sensing on the basis of solvation effects and were measured by using TSM resonators (96, 105). These films had a hydrophilic structure that gave them a high affinity for polar solvent vapors (106). The plasma-polymerized films contained unsaturated carbon moieties available for interactions with small organic molecules using π -electrons and unpaired electrons. In addition, the unsaturated radical sites in the carbon networks were suitable for enhancement of mobility of highly cross-linked carbon networks, making them effective at solvating small organic molecules (107). The effects of adsorbed/absorbed water on the response of these plasma polymer films on TSM resonators were further explored (96). Water sorbed on these films before chemical exposure played a significant role involving hydrophilic/hydrophobic interactions between investigated vapors, sorbed water, and the sensing films.

3.2. Biomolecule-Functionalized Nanomaterials

Diverse nanomaterial types such as CNTs, graphene, semiconducting inorganic nanowires, semiconducting conjugated polymer nanotubes, and metal nanoparticles have been used as transducing nanomaterial elements and have been functionalized with biomolecules (108–114). Biomolecules implemented for the functionalization of nanomaterials include single-stranded DNA (109), single-stranded RNA (115), peptides (114, 116), and olfactory receptor proteins

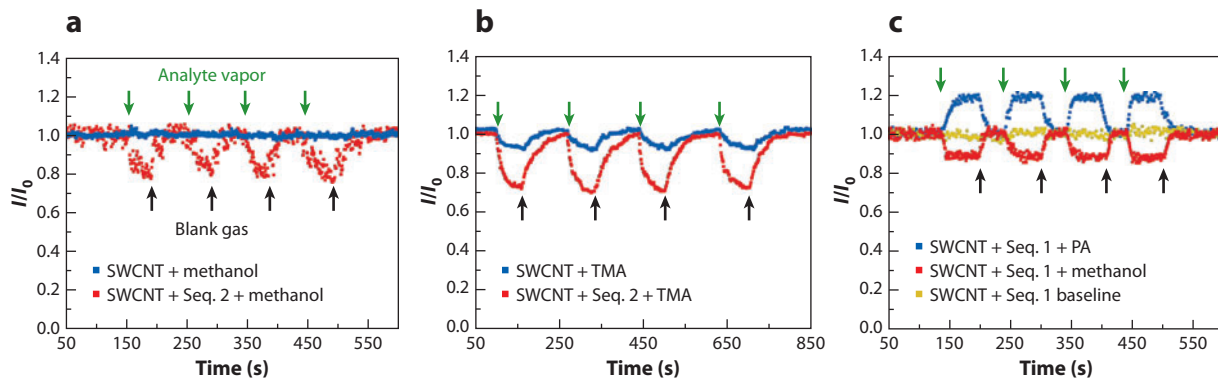


Figure 10

Response of field effect transistor transducers with DNA-functionalized single-walled carbon nanotubes (SWCNTs) to diverse vapors. The sensor current was normalized to the sensor response in blank air. (a) The response of bare (blue points) and functionalized (red points) SWCNTs to 4,000 ppm of methanol. DNA sequence: 5' CTT CTG TCT TGA TGT TTG TCA AAC 3'. (b) Response of bare (blue points) and functionalized (red points) SWCNTs to 20,000 ppm of trimethylamine. DNA sequence: 5' CTT CTG TCT TGA TGT TTG TCA AAC 3'. (c) Response of functionalized SWCNTs to 150 ppm of propionic acid (blue points) and 4,000 ppm of methanol (red points), with the current baseline shown with yellow points. DNA sequence: 5' GAG TCT GTG GAG GAG GTA GTC 3'. Green and black arrows in panels a–c show the introduction of an analyte vapor and a blank gas, respectively. Abbreviations: PA, propionic acid; TMA, trimethylamine. Adapted with permission from Reference 109.

(117). Different physical transducers such as FETs (108, 109) and resonators (118) have been implemented for the detection of vapor responses. Such a combination of biomolecule-based sensing moieties and the different types of transducing nanomaterials and physical transducers promises to enhance vapor selectivity compared with sensing by using more traditional sensing materials.

At present, CNTs and graphene are the most popular carbon allotropes under investigation as vapor-sensing materials (4). Unlike other sensing materials, all atoms in CNTs and graphene are surface atoms; thus, electron transport through these materials can be efficiently modulated by the environment around these atoms, including adsorbed vapor molecules. However, unless properly functionalized, these materials suffer from nonselective vapor responses. Inspired by the covalent and noncovalent functionalization of CNTs with biomolecules (119, 120) applicable for biosensing in the aqueous phase, functionalization of CNTs with biomolecules to perform vapor-phase sensing has also attracted significant attention. Single-stranded DNA-functionalized CNT films on FET transducers responded to vapors that did not cause a detectable conductivity change in bare CNT devices (109). Responses were reversible and different in direction and magnitude for different vapors and were tuned by choosing the base sequence of DNA molecules (see **Figure 10**) (109). DNA-functionalized sensors have been further used for the detection of a homologous series of aldehydes and carboxylic acids commonly found in human breath and other body emanations (121). To better understand the nature of DNA-CNT self-assembly during the functionalization of sensing films, the DNA base–CNT binding free energies were computed for all four DNA bases in aqueous solution at room temperature (122). The affinities of the DNA bases for CNT binding followed the trend $G > A > T > C$, with the base-CNT interactions dominated by π - π stacking interactions with a solvent. CNT-DNA films deposited on resonant transducers were further demonstrated for the detection of DNT and dimethyl methylphosphonate (DMMP) (118). The selectivity of vapor determinations was further tested not only with CNT-DNA films but also with CNT-RNA films (115). These studies demonstrated the ability of these films deposited

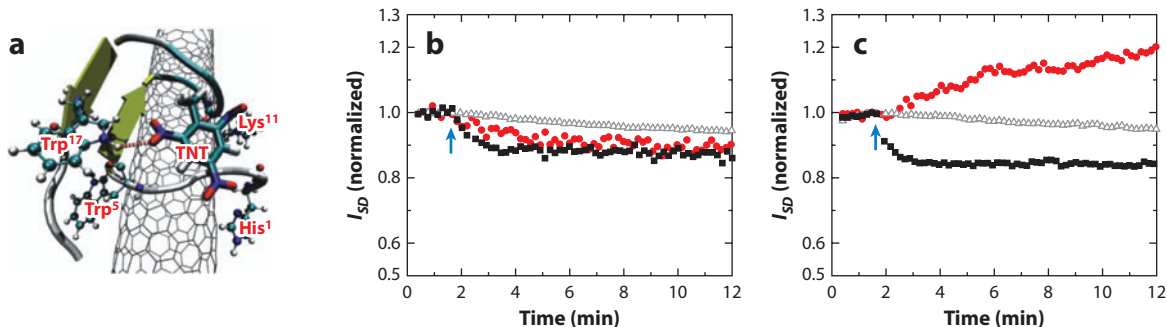


Figure 11

Peptide-functionalized single-walled carbon nanotubes (SWCNTs) for the detection of explosives. (a) Computational model of TNT binding to a PIASPIC-SWCNT hybrid through a H bond with Trp¹⁷ and a π - π interaction with the SWCNT surface. Response of (b) bare SWCNT and (c) PIASPIC-coated SWCNT transducer to TNT (red circles), RDX (gray triangles), and HPT (black squares). Blue arrows in panels b and c show introduction of analyte vapors. Abbreviations: HPT, 2-heptanone; RDX, cyclotrimethylenetrinitramine; TNT, trinitrotoluene. Adapted with permission from Reference 108.

onto FETs to discriminate between structural isomers, pairs of enantiomers, and members of a homologous series of vapor-phase analytes differing by single methylene units.

Peptides have also been employed for the functionalization of CNTs (108). Peptide vapor-recognition elements were rationally designed to perform two functions at once: noncovalent attachment to CNTs and binding to TNT as the model vapor analyte (123). The peptide-recognition elements contained two domains: a TNT-binding domain derived from the binding pocket of the honeybee odor-binding protein and a CNT-binding peptide identified from the phage peptide display library. The odor-binding protein contained a C-terminal tail fragment that binds to pheromones and other chemical targets. Four amino acids residues (Trp-Phe-Val-Ile) at the C terminus played an important role in binding to TNT. Computations of interactions between the peptide-CNT hybrid and three different chemical agents [TNT, cyclotrimethylenetrinitramine (RDX), and 2-heptanone (HPT)] demonstrated that RDX and HPT did not bind strongly to the peptide. However, TNT bound to the peptide via the nitro group of TNT, forming a hydrogen bond with Trp¹⁷, whereas the ring of TNT stacked on the surface of the CNT (see **Figure 11a**), providing a binding motif for TNT to the peptide-CNT hybrid (108). The bare CNT and peptide-CNT sensors were further exposed to TNT, RDX, and HPT vapors (see **Figure 11b,c**). The peptide-functionalized CNT-FET exhibited a selective response to TNT, as evidenced by the signal increase upon exposure to TNT, whereas the bare CNT-FET responded with a signal decrease. RDX and HPT vapor exposures showed no selectivity because the signal changes were similar for both bare and functionalized SWCNT-FET devices.

Single-stranded DNA molecules that were initially applied to functionalize CNTs (109) were further applied to functionalize graphene for the detection of DMMP and propionic acid (110). For both model analyte vapors, the current response of clean graphene was very low and barely detectable above system noise. After coating with single-stranded DNA, 5–50% response enhancements were observed. Similar to the role of single-stranded DNA-CNT sensors (109), the role of the single-stranded DNA was to concentrate water and analyte molecules near the otherwise chemically inert and hydrophobic conduction channel and, in this way, to increase the current response compared with that of bare graphene.

Besides carbon allotropes such as CNTs and graphene, other organic nanomaterials have also been implemented for functionalization with biomolecules for vapor sensing. Carboxylated

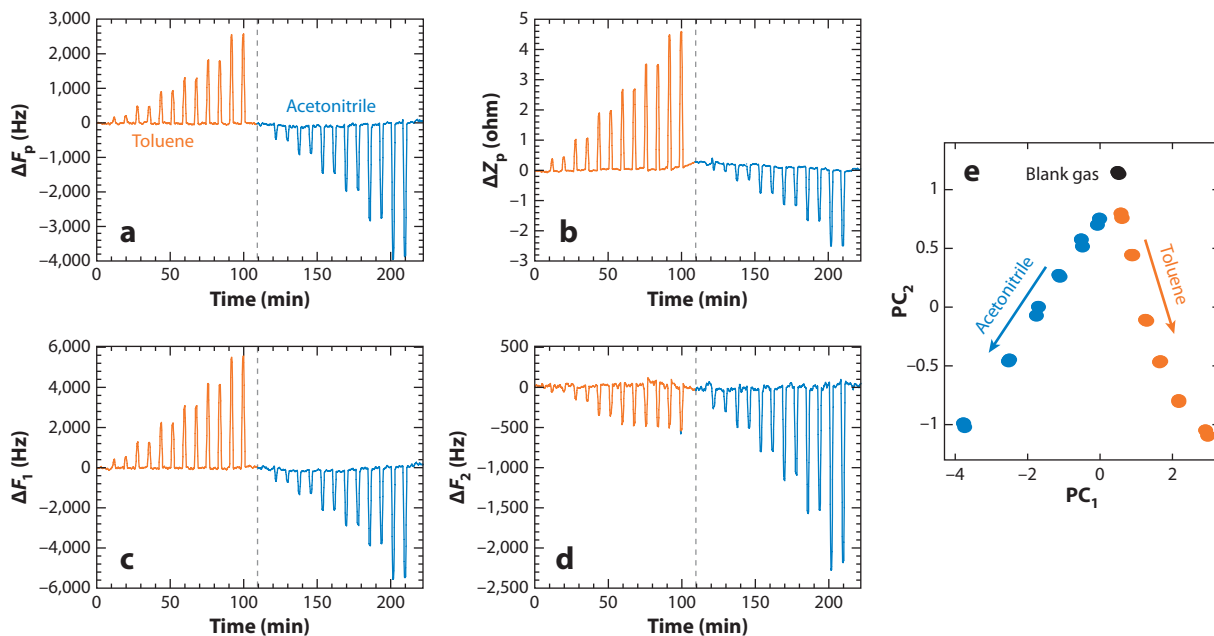


Figure 12

Response of an individual multivariable sensor to representative vapors (toluene and acetonitrile). Panels *a–d* show F_p , Z_p , F_1 , and F_2 responses, respectively. Concentrations of vapors are 0, 0.02, 0.04, 0.07, 0.10, 0.15, and 0.2 P/P_0 . The sensor is exposed to replicate $n = 2$ concentrations of each vapor. (*e*) The designed response diversity of a single multivariable sensor to two representative vapors (toluene and acetonitrile). Shown is a scores plot of the first two principal components (PCs) of a principal-components-analysis model. Adapted with permission from Reference 59.

polypyrrole nanowires were functionalized with human olfactory receptor protein for the detection of gaseous odorants such as helional at concentrations as low as 0.02 parts per trillion (111).

Inorganic semiconducting nanomaterials have also been implemented for functionalization with biomolecules for vapor sensing. Silicon nanowires were used as a substrate for covalent attachment of polypeptides for studies of vapor-phase responses to ammonia and acetic acid by using a FET transducer (112). Selectivity of peptides to ammonia and acetic acid in dry carrier gas was achieved from the combination of acid/base reactivity and the molecular structure of peptides.

The biomolecular functionalization of metal nanoparticles for vapor sensing is much less explored than the biofunctionalization of CNTs, graphene, and nanowires. Typically, monolayer-capped metal nanoparticles are employed with resistor (124), capacitor (125), and TSM (22) transducers. With resistor and capacitor transducers, the film resistance and capacitor changes are related to (*a*) electron tunneling between metal cores through the dielectric ligand shell and to (*b*) charge hopping along the atoms of the dielectric ligand shell (23). With TSM transducers, the mass change of the film is related to vapor sorption into the dielectric ligand shell of the monolayer-capped metal nanoparticles (22). Sensor response diversity is achieved by designing different ligands for metal nanoparticles with soft and rigid linkers. The soft linkers change their length as a function of the amount of sorbed vapor. Rigid linkers restrain swelling of sensing films and boost the effects of analyte-dependent changes of the dielectric constant of the film.

To demonstrate performance capability of multivariable sensors with monolayer-capped metal nanoparticles, **Figure 12** illustrates an LCR sensor response with an organothioli-functionalized metal nanoparticle film by using toluene and acetonitrile (ACN) as model vapors (59). Four

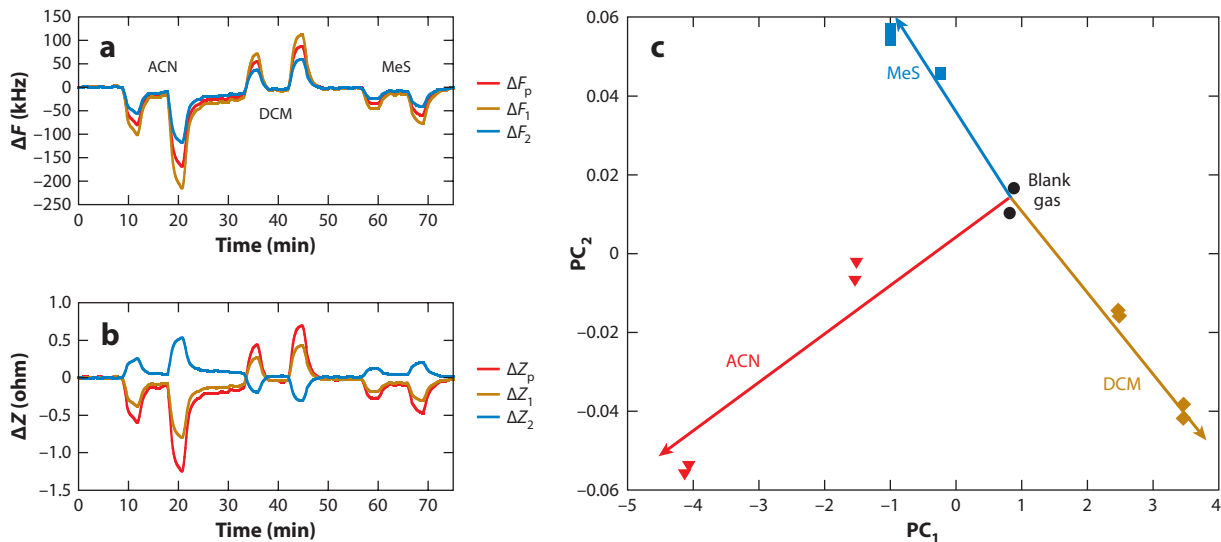


Figure 13

Discrimination of vapors using an individual multivariable resonant inductor-capacitor-resistor transducer with A3 peptide-capped gold nanoparticles. (a) Sensor responses F_p , F_1 , and F_2 . (b) Sensor responses Z_p , Z_1 , and Z_2 . (c) Scores plot of a principal-components-analysis (PCA) model of a sensor response with replicate ($n = 2$) data points for each concentration. The first two principal components (PCs) of the built PCA model of the response of the A3-Au nanoparticle material to dichloromethane (DCM), acetonitrile (ACN), and methyl salicylate (MeS) vapors included more than 99% of the total variance from the data set. Concentrations of vapors were 0.044 and 0.089 P/P_0 . The water vapor background was at $P/P_0 = 0.18$. Adapted from Reference 113.

measured parameters, F_p , Z_p , F_1 , and F_2 , were extracted from the measured resonance impedance of the sensor (**Figure 12a–d**) and provided a strong response pattern of sensor upon exposure to these two vapors. This response diversity was pronounced in the response direction and magnitude for each vapor. For example, the F_p , F_1 , and Z_p responses had opposite directions for two vapors, whereas the F_2 response showed a similar direction. Response magnitudes also varied significantly in the measured F_p , Z_p , F_1 , and F_2 parameters. In particular, the Z_p response to toluene was approximately twofold stronger than that to ACN. At the same time, the F_2 response to toluene was threefold weaker than that to ACN. This response diversity was due to the nature of the sensing film and sensor design. The response pattern from this single sensor was further analyzed by using PCA (**Figure 12e**). These results illustrate strong discrimination between these two vapors obtained with this single sensor.

The applicability of biological capping ligands to gold nanoparticles was recently demonstrated for selective vapor detection through the use of an individual multivariable LCR transducer and the A3 peptide AYSSGAPPMPFF as the biological capping ligand (113). As model analytes, toxic vapors and chemical warfare agent simulants, such as ACN, dichloromethane (DCM), and methyl salicylate (MeS), were used (**Figure 13**). The direction of the sensor response to DCM was opposite of that of the response to MeS vapor (**Figure 13a,b**), even though DCM has a dielectric constant $\epsilon_r = 9.1$, which is close to that of MeS ($\epsilon_r = 9.0$). However, MeS is much bulkier than DCM, and this increased bulkiness may therefore affect the rigidity of the linker differently, as reflected in the measured resonant spectral response. Results of multivariate PCA analysis (**Figure 13c**) illustrated the discrimination ability provided by this single A3-Au nanoparticle material. The PCA model was built by using six (F_p , F_1 , F_2 , Z_p , Z_1 , and Z_2) responses from the sensor. The single multivariable sensor was able to discriminate three types of vapors, including DCM and

Table 2 Mechanisms of structural coloration in animals (131–136)

Scattering	Interference	Diffraction	Combined effects
<ul style="list-style-type: none"> ■ Wing scales of <i>Papilio zalmoxis</i> butterfly ■ Wing scales of <i>Parides sesostris</i> butterfly ■ Abdomen of <i>Amenia</i> fly ■ Cuticle of <i>Orthetrum caledonicum</i> dragonfly ■ Skin of <i>Octopus bimaculatus</i> cephalopod marine mollusk ■ Wings of <i>Libellula pulchella</i> dragonfly 	<ul style="list-style-type: none"> ■ Cicindelid cuticle of tiger beetles ■ Golden pupae of danaine butterflies ■ Cuticle of <i>Limnadia</i> clam shrimp ■ Cuticle of a swimming paddle of <i>Ovalipes molleri</i> crab ■ Eyes of <i>Pecten</i> scallop ■ Neck features of rock dove 	<ul style="list-style-type: none"> ■ Wing scales of green hairstreak (<i>Callophrys rubi</i>) butterfly ■ Antenna of <i>Azygocypridina lowryi</i> seed shrimp ■ Junctions between rows of cells in indigo snakes ■ Elytra of burying and gyrinid beetles ■ Seta of <i>Lobochesis longiseta</i> polychaete worms ■ Blazed gratings on wing scales of <i>Plusia argentifera</i> moth 	<ul style="list-style-type: none"> ■ Surface of elytra of male beetles <i>Chlorophila obscuripennis</i> comprises a sculpted multilayer resulting in blue iridescence from regularly spaced indentations and in green iridescence from the ridges surrounding the indentations ■ Wing scales of <i>Morpho</i> butterflies exhibit combined diffraction and interference optical effects due to the coexistence of a periodic ridge structure with multilayers of lamella

MeS vapors, with very similar dielectric constants. This new type of sensing materials can provide numerous opportunities for tailoring the vapor-response selectivity on the basis of the diversity of the amino acid composition of the peptides and by modulating the nature of peptide-nanoparticle interaction through designed combinations of hydrophobic and hydrophilic amino acids.

4. VAPOR SENSING WITH BIOINSPIRED NANOSTRUCTURES

Numerous natural biological nanostructures have become the focus of growing attention for sensing applications. This interest is driven by the design features of these nanostructures that often provide geometries that are difficult or impossible to reproduce by using existing nanofabrication tools. Reported transduction principles using bioinspired nanostructures include optical (65–69, 126–128) and electrical (129, 130) transducers.

Numerous biological structures exhibit structural color based on the formation of natural photonic crystals. These photonic crystals are 1-D, 2-D, and even 3-D structures (131) and are related to a phenomenon of structural color across the animal kingdom that has been under development for more than 500 million years (132). **Table 2** presents examples of natural photonic structures that demonstrate different types of interactions with light such as scattering, diffraction, interference, and their combination (131–136). These results illustrate a vast diversity of approaches taken by natural structures to produce structural colors.

Some photonic structures in nature exhibit intrinsic vapor responses. For example, a *Dynastes hercules* beetle displays a diffractive hygrochromic effect, changing its color from green to black upon an increase in the moisture content in air above 80% (137). Several photonic natural structures, such as scales of butterflies (65–67, 138), scales of beetles (137), and bird feathers (68), have been studied for their vapor responses, with the goal of exploring the physics of the optical effects, selectivity, and sensitivity of vapor responses.

4.1. Vapor Responses of Biological Structures

Recently, iridescent scales of *Morpho* butterflies were demonstrated as “sensing materials” that provided an unexpected diverse optical response to different vapors (65). In these butterfly scales, the lamellae of the scale ridges act as multilayer interferometric nanoreflectors, whereas the ridges

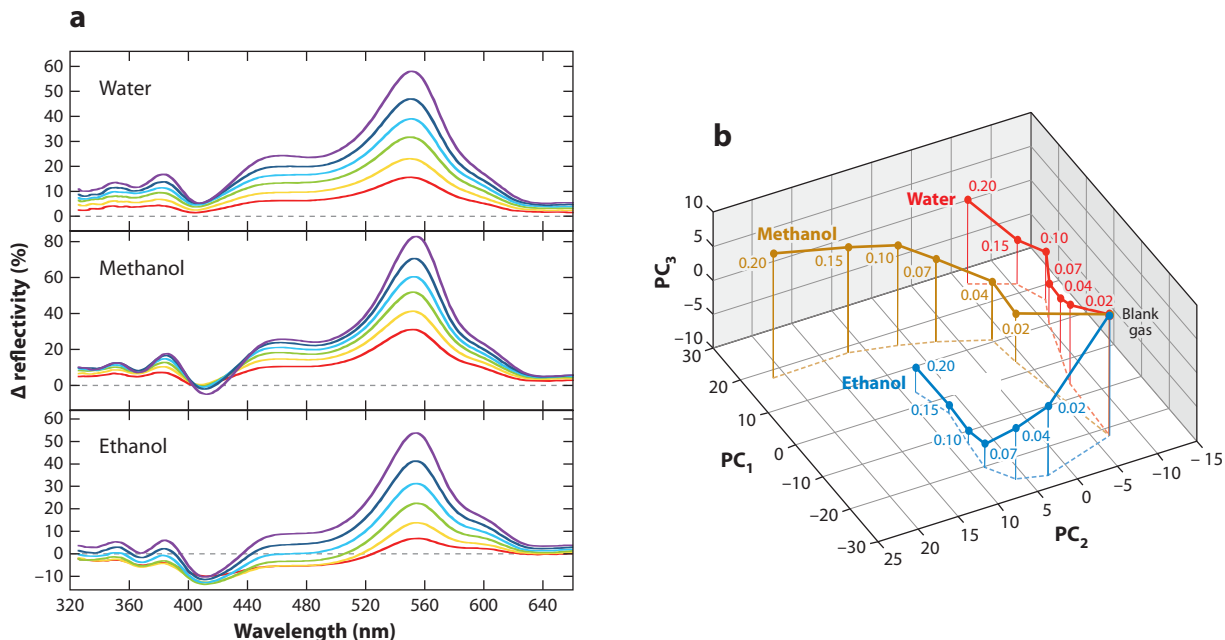


Figure 14

Analysis of selectivity of spectral response of the photonic structure of *Morpho sulkowskyi* to different vapors. (a) Differential reflectance spectra upon exposure to water, methanol, and ethanol vapors of increasing partial pressure ranging from 0 to 0.2 P/P_0 . Vapor concentrations were 0 (black lines), 0.02 (red curves), 0.04 (yellow curves), 0.07 (green curves), 0.1 (light-blue curves), 0.15 (dark-blue curves), and 0.2 (purple curves) P/P_0 . (b) Discrimination of water, methanol, and ethanol vapors using principal-components analysis (PCA).

Adapted with permission from Reference 65.

of the scales act as a diffraction grating, together combining multilayer interference from individual reflectors and diffraction from the array of these reflectors (133). Spectral measurements of the scales in the visible range provide information about the nature and concentration of the vapors, allowing for the identification of closely related vapors such as water, methanol, and ethanol with a single sensing structure. The chemical selectivity of response of these photonic structures was examined by exposing an $\sim 5 \times 5$ -mm region of the wing to a variety of vapors presented individually at different concentrations and by monitoring the differential reflectance spectra. **Figure 14a** illustrates the differential reflectance spectra of scales upon exposure to water, methanol, and ethanol vapors. The differential reflectance response patterns of the scales to these closely related vapors were very diverse. The most pronounced spectral differences were at 325–500 nm and in response magnitude at 500–600 nm. To differentiate these responses quantitatively, multivariate spectral analysis such as PCA was applied (**Figure 14b**). PCA demonstrated that three tested vapors were perfectly differentiated, even at the lowest tested vapor partial pressure.

4.2. Structurally Colored Colloidal Crystal Films Based on Core/Shell Nanospheres

The 3-D-ordered arrays of colloidal nanoparticles with cubic-close-packed or face-center-cubic structures are very common in nature as natural opals and inspire numerous technological applications (139). Artificial self-assembled structures based on the principles of natural opals have been

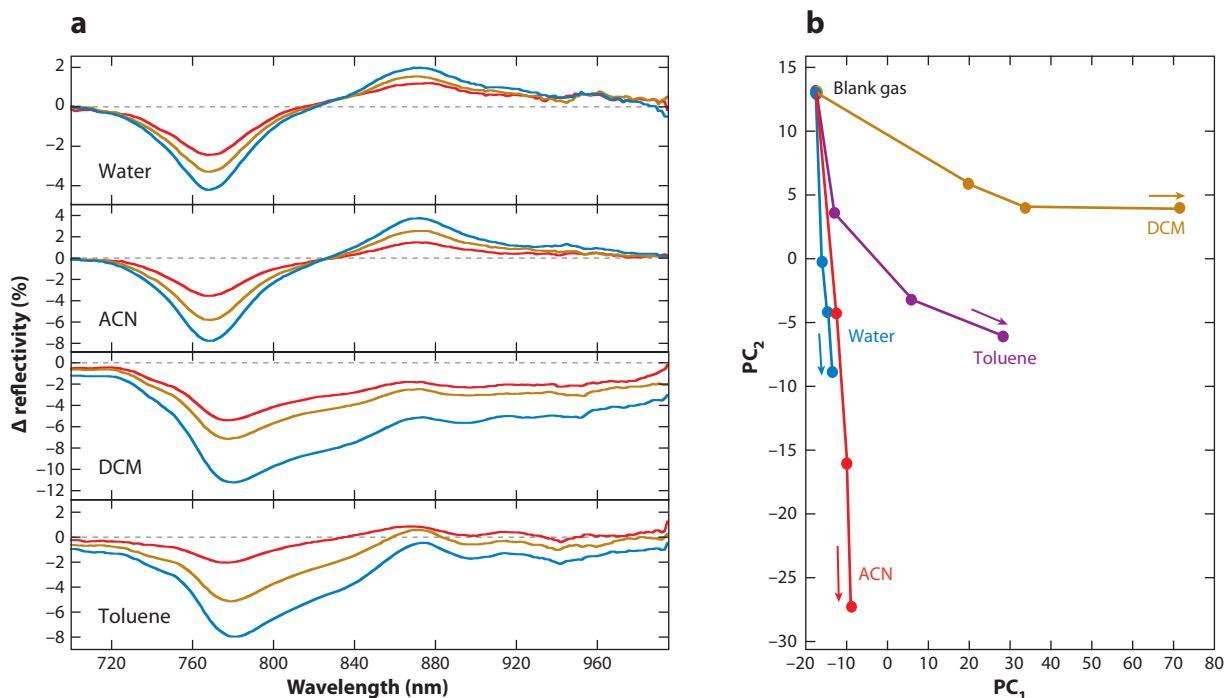


Figure 15

Selective detection of vapors using a single structurally colored colloidal crystal film formed from composite core/shell nanospheres. (a) Differential reflectance spectra for four vapors [water, acetonitrile (ACN), dichloromethane (DCM), and toluene] of increasing partial pressure ranging from 0 to 0.07 P/P_0 . Vapor concentrations are 0 (gray dashed lines), 0.02 (red curves), 0.04 (gold curves), and 0.07 (blue curves) P/P_0 . (b) The multivariate response of the colloidal sensor film for four tested vapors. Multivariate analysis was done by using PCA tools by processing differential reflectance spectra over the 700–995-nm range. Arrows indicate the increase in concentrations of each vapor. Vapor concentrations are 0, 0.02, 0.04, and 0.07 P/P_0 . Adapted with permission from Reference 64.

extensively used for chemical sensing (64, 140–143). Traditionally, for monitoring of multiple analytes, individual photonic crystal sensing films are combined in an array in which each film has partial response selectivity to a certain class of analytes (142). To reduce or even overcome the need for the construction of sensor arrays, selective sensing of multiple vapors was demonstrated on the basis of the structurally colored colloidal crystal films formed from composite core/shell nanospheres (with a 326-nm-diameter polystyrene core and a 20-nm-thick sol-gel shell) (64). The vapor-sensing selectivity was provided by the combination of (a) the composite nature of the colloidal nanospheres in the film and (b) multivariate analysis of the spectral changes in the film reflectivity upon exposure to different vapors. In these sensors, the detection mechanism is based on the change in the optical lattice constant of the colloidal crystal arrays as a function of analyte concentration; such a change leads to the variation in the shape of the Bragg diffraction band. To evaluate the response of the sensor, several model vapors of different polarity such as water, ACN, DCM, and toluene were selected (Figure 15). Changes in the differential reflectance spectra of the sensing film upon exposure to different vapors at various concentrations illustrate several important findings (Figure 15a). For polar vapors such as water and ACN, the differential reflectance spectra have a stable baseline and consistent well-behaved changes in the reflectivity as a function of analyte concentration. The response of the colloidal crystal film to nonpolar vapors such as DCM and toluene is quite different from the response to polar vapors. There are

pronounced analyte concentration–dependent baseline offsets that are likely due to the distortions of the optical lattice upon exposure to nonpolar vapors. These distortions are likely caused by the reversible slight swelling of the core of the nanospheres by the vapors. Discrimination of vapors using a single sensing colloidal crystal film was done through PCA (**Figure 15b**). The best selectivity was obtained between toluene and DCM vapors, whereas water and ACN vapors were almost unresolved.

5. MAJOR DIRECTIONS IN DEVELOPMENT AND APPLICATION SCENARIOS

The current and intended future implementations of vapor sensors can be summarized as installations into stationary infrastructure (e.g., interiors of residential and commercial buildings, industrial infrastructure), integration into nonstationary platforms (e.g., desktop analytical instrumentation, transportation vehicles, home appliances), integration into handheld or wearable components (e.g., pocket detectors, mobile phones, active wear), and single-use installations (e.g., medical and food packaging). The acceptance of vapor sensors deployed in these implementations relies on the ongoing and future technological advances toward new broad application scenarios such as (a) wireless sensing, (b) battery-independent sensor operation, (c) distributed sensor networks, and (d) unobtrusive sensor designs.

5.1. Wireless Sensing

The trend toward wireless sensing is driven by several key advantages of wireless sensors over traditional tethered sensors. Benefits of wireless sensors include the unobtrusive nature of sensor installations, higher nodal densities, and lower installation costs without the need for extensive wiring. Depending on the sensor design and mode of operation, wireless sensors can be categorized as active and passive. Active wireless sensors have on-board power to perform sensing and signal transmission. Passive wireless sensors lack on-board power and receive their power from the electromagnetic field generated by the sensor reader. Wireless sensors that adapt wireless communication concepts originally developed for radio-frequency identification (RFID) tags are also known as RFID sensors (144), with growing interest in the application of near-field communication protocols for wireless sensing (60). Most of the transducers that have been developed have also been implemented in wireless sensors (4).

5.2. Battery-Independent Sensor Operation

The trend toward battery-independent sensor operation is driven by opportunities that could be provided in sensor operation without the need for a battery and is inspired by the technological advances in the area of power scavenging (harvesting) (145, 146). At present, the power consumption of the most widely used vapor sensors, such as metal oxide semiconductor (MOS) sensors, is 30–400 mW (147, 148). Although such power requirements are often not an issue for tethered sensor implementations, they are unacceptable for the long-term wireless installations of sensors. Thus, sensors that require much less or no on-board power and simultaneously provide the same performance as or better performance than available MOS sensors are highly desired and are under development, including those with self-heating capabilities (149). With the reduction of required power for sensor operation, new opportunities arise to harvest power from the available ambient sources.

To properly assess the power requirements for a wireless vapor sensor, it is critical to take into the account not only the power needed for the operation of different transducers, but

also the power needed for the operation of the wireless transmitter. Different types of energy-harvesting devices provide different amounts of energy, e.g., from an ambient radio-frequency background ($\sim 0.001 \text{ mW cm}^{-2}$), human/industrial motion and vibrations ($0.005\text{--}0.5 \text{ mW cm}^{-2}$), human/industrial heat ($0.05\text{--}10 \text{ mW cm}^{-2}$), and indoor/outdoor light ($0.01\text{--}50 \text{ mW cm}^{-2}$) (145, 146). Depending on the desired wireless communication distance, data rate, and other specifications, the needed power for a typical distance of wireless communication is, for example, 30 mW (ZigBee, 10–75 m), 2.5–100 mW (Bluetooth, 10–100 m), and 25 μW (MICS, ~ 2 m) (150).

5.3. Distributed Sensor Networks

Arranging individual sensors into a distributed set to form a sensor network is gaining acceptance for a wide variety of sensing applications, including vapor sensing, in which sensors are implemented in their wireless configurations (60, 151, 152). Wireless sensor networks (WSNs) provide valuable spatially resolved, distributed information that cannot be obtained by using tethered sensors. One of the most critical challenges of WSNs for vapor sensing is the power consumption of individual sensors (see Section 5.2). Another critical challenge of WSNs for vapor sensing is the insufficient selectivity of existing sensors and sensor arrays (4). As in conventional tethered sensor systems, minimizing the number of wireless sensors in an array is attractive because it simplifies data analysis, reduces data-processing noise, and simplifies sensor material deposition and device fabrication. However, for a wireless sensor node device, minimizing the number of sensors in an array brings the additional critical benefit of minimizing the required power.

5.4. Unobtrusive Sensor Designs

The trend toward unobtrusive sensor designs is driven by opportunities that could be provided in the operation of sensors that are either micro- or nanosized, flexible, or fabric integrated. This trend is inspired by technological advances in the areas of sensor nanofabrication (153), flexible (154, 155) and stretchable (156) sensors, and printed/flexible electronics (154, 157). Potential applications of such unobtrusive sensor designs range from implanted and in vivo sensors (114) to smart tattoo (156) and smart food label (158, 159) sensors to wearable sensors (150) with different sensor-readout methods, including readout of multivariable electronic (160) and optical (161) sensors in smartphone and other mobile devices.

6. OUTLOOK

To achieve vapor-response selectivity of sensors desired for numerous applications, it is critical to combine the proper materials with a multivariable transducer. Such combination provides the ability to perform selective vapor measurements without the need for a sensor array. Such simplification of the sensor system design becomes important for applications in which power requirements, manufacturability, and unobtrusive sensor design are critical. The two new types of sensing materials described here, bionanomaterials and bioinspired nanostructures, have the strong potential to significantly improve selectivity of field-operated sensors. The materials critically reviewed here are compatible with different types of transducers, providing the ability to tune the sensor design to certain practical implementations in which the type of sensor readout is important, for example, for visual self-reporting sensors and for integration with existing electronic device infrastructure.

DISCLOSURE STATEMENT

The authors are not aware of any affiliations, memberships, funding, or financial holdings that might be perceived as affecting the objectivity of this review.

ACKNOWLEDGMENTS

The research from GE and Air Force Research Laboratory (AFRL) cited here was performed by the creative members of teams that coauthored the original contributions cited here. The authors acknowledge J. Cournoyer (GE Global Research) for providing the scanning electron microscopy images in **Figure 8**. This work was supported in part by GE corporate fundamental research funds, by the National Institute of Environmental Health Sciences (grant number 1R01ES016569-01A1), by the Defense Advanced Research Projects Agency (contract W911NF-10-C-0069), and by AFRL (contract FA8650-08-C-6869). R.R.N. acknowledges support from the Air Force Office of Scientific Research and from the Materials and Manufacturing Directorate.

LITERATURE CITED

1. Potyrailo RA, Mirsky VM. 2008. Combinatorial and high-throughput development of sensing materials: the first ten years. *Chem. Rev.* 108:770–813
2. Mirsky VM, Yatsimirsky AK, eds. 2011. *Artificial Receptors for Chemical Sensors*. Weinheim, Ger.: Wiley-VCH
3. Fitch JP, Raber E, Imbro DR. 2003. Technology challenges in responding to biological or chemical attacks in the civilian sector. *Science* 302:1350–54
4. Potyrailo RA, Surman C, Nagraj NN, Burns A. 2011. Materials and transducers toward selective wireless gas sensing. *Chem. Rev.* 111:7315–54
5. Collins PG, Bradley K, Ishigami M, Zettl A. 2000. Extreme oxygen sensitivity of electronic properties of carbon nanotubes. *Science* 287:1801–4
6. Schedin F, Geim AK, Morozov SV, Hill EW, Blake P, et al. 2007. Detection of individual gas molecules adsorbed on graphene. *Nat. Mater.* 6:652–55
7. Chen G, Paronyan TM, Harutyunyan AR. 2012. Sub-ppt gas detection with pristine graphene. *Appl. Phys. Lett.* 101:053119
8. Potyrailo RA. 2006. Polymeric sensor materials: toward an alliance of combinatorial and rational design tools? *Angew. Chem. Int. Ed.* 45:702–23
9. Grate JW. 2008. Hydrogen-bond acidic polymers for chemical vapor sensing. *Chem. Rev.* 108:726–45
10. Hierlemann A, Gutierrez-Osuna R. 2008. Higher-order chemical sensing. *Chem. Rev.* 108:563–613
11. Middelhoek S, Noorlag JW. 1981/82. Three-dimensional representation of input and output transducers. *Sens. Actuators* 2:29–41
12. Potyrailo RA, Leach AM, Morris WG, Gamage SK. 2006. Chemical sensors based on micromachined transducers with integrated piezoresistive readout. *Anal. Chem.* 78:5633–38
13. Kirchner P, Oberländer J, Friedrich P, Berger J, Rysstad G, et al. 2012. Realisation of a calorimetric gas sensor on polyimide foil for applications in aseptic food industry. *Sens. Actuators B* 170:60–66
14. Sugiyasu K, Swager TM. 2007. Conducting-polymer-based chemical sensors: transduction mechanisms. *Bull. Chem. Soc. Jpn.* 80:2074–83
15. Li B, Santhanam S, Schultz L, Jeffries-EL M, Iovu MC, et al. 2007. Inkjet printed chemical sensor array based on polythiophene conductive polymers. *Sens. Actuators B* 123:651–60
16. Di Natale C, Paolesse R, D'Amico A. 2007. Metalloporphyrins based artificial olfactory receptors. *Sens. Actuators B* 121:238–46
17. Pirondini L, Dalcanale E. 2007. Molecular recognition at the gas-solid interface: a powerful tool for chemical sensing. *Chem. Soc. Rev.* 36:695–706
18. Pinalli R, Suman M, Dalcanale E. 2004. Cavitands at work: from molecular recognition to supramolecular sensors. *Eur. J. Org. Chem.* 2004:451–62

19. Yan Y, Bein T. 1992. Molecular recognition on acoustic wave devices: sorption in chemically anchored zeolite monolayers. *J. Phys. Chem.* 96:9387–93
20. MacGillivray LR, ed. 2010. *Metal-Organic Frameworks: Design and Application*. Hoboken, NJ: Wiley
21. Kreno LE, Leong K, Farha OK, Allendorf M, Van Duyne RP, Hupp JT. 2012. Metal-organic framework materials as chemical sensors. *Chem. Rev.* 112:1105–25
22. Grate JW, Nelson DA, Skaggs R. 2003. Sorptive behavior of monolayer-protected gold nanoparticle films: implications for chemical vapor sensing. *Anal. Chem.* 75:1868–79
23. Steinecker WH, Rowe MP, Zellers ET. 2007. Model of vapor-induced resistivity changes in gold-thiolate monolayer-protected nanoparticle sensor films. *Anal. Chem.* 79:4977–86
24. Snow ES, Perkins FK, Houser EJ, Badescu SC, Reinecke TL. 2005. Chemical detection with a single-walled carbon nanotube capacitor. *Science* 307:1942–45
25. Bondavalli P, Legagneux P, Pribat D. 2009. Carbon nanotubes based transistors as gas sensors: state of the art and critical review. *Sens. Actuators B* 140:304–18
26. Hierlemann A, Ricco AJ, Bodenhöfer K, Göpel W. 1999. Effective use of molecular recognition in gas sensing: results from acoustic wave and in situ FT-IR measurements. *Anal. Chem.* 71:3022–35
27. De Souza JEG, Dos Santos FL, Neto BB, Dos Santos CG, Dos Santos MVB, De Melo CP. 2003. Free-grown polypyrrole thin films as aroma sensors. *Sens. Actuators B* 88:246–59
28. Pinalli R, Nachtigall FF, Ugozzoli F, Dalcanale E. 1999. Supramolecular sensors for the detection of alcohols. *Angew. Chem. Int. Ed.* 38:2377–80
29. Marr I, Reiß S, Hagen G, Moos R. 2011. Planar zeolite film-based potentiometric gas sensors manufactured by a combined thick-film and electroplating technique. *Sensors* 11:7736–48
30. Sarkisov L. 2012. Toward rational design of metal-organic frameworks for sensing applications: efficient calculation of adsorption characteristics in zero loading regime. *J. Phys. Chem. C* 116:3025–33
31. Dua V, Surwade SP, Ammu S, Agnihotra SR, Jain S, et al. 2010. All-organic vapor sensor using inkjet-printed reduced graphene oxide. *Angew. Chem. Int. Ed.* 49:2154–57
32. Persaud K, Dodd G. 1982. Analysis of discrimination mechanisms in the mammalian olfactory system using a model nose. *Nature* 299:352–55
33. Jurs PC, Bakken GA, McClelland HE. 2000. Computational methods for the analysis of chemical sensor array data from volatile analytes. *Chem. Rev.* 100:2649–78
34. Hagleitner C, Hierlemann A, Lange D, Kummer A, Kerness N, et al. 2001. Smart single-chip gas sensor microsystem. *Nature* 414:293–96
35. Ulmer H, Mitrovics J, Weimar U, Göpel W. 2000. Sensor arrays with only one or several transducer principles? The advantage of hybrid modular systems. *Sens. Actuators B* 65:79–81
36. Wiziack NKL, Catini A, Santonico M, D'Amico A, Paolesse R, et al. 2009. A sensor array based on mass and capacitance transducers for the detection of adulterated gasolines. *Sens. Actuators B* 140:508–13
37. Wang Y, Yu K, Wang D, Zhao C, Wang L, Wang P. 2011. Multi-model diagnosis method for lung cancer based on MOS-SAW breath detecting e-nose. *AIP Conf. Proc.* 1362:163–64
38. Dickson JA, Goodman RM. 2000. Integrated chemical sensors based on carbon black and polymer films using a standard CMOS process and post-processing. *Proc. IEEE Int. Symp. Circuits Syst.* 4:341–44
39. Beccherelli R, Zampetti E, Pantalei S, Bernabei M, Persaud KC. 2010. Design of a very large chemical sensor system for mimicking biological olfaction. *Sens. Actuators B* 146:446–52
40. Deleted in proof
41. Aernecke MJ, Walt DR. 2009. Optical-fiber arrays for vapor sensing. *Sens. Actuators B* 142:464–69
42. Oprea A, Courbat J, Briand D, Bârsan N, Weimar U, De Rooij NF. 2012. Environmental monitoring with a multisensor platform on polyimide foil. *Sens. Actuators B* 171–172:190–97
43. Röck F, Bârsan N, Weimar U. 2008. Electronic nose: current status and future trends. *Chem. Rev.* 108:705–25
44. Snow ES, Perkins FK. 2005. Capacitance and conductance of single-walled carbon nanotubes in the presence of chemical vapors. *Nano Lett.* 5:2414–17
45. Torsi L, Dodabalapur A, Sabbatini L, Zamboni PG. 2000. Multi-parameter gas sensors based on organic thin-film-transistors. *Sens. Actuators B* 67:312–16

46. Meier DC, Raman B, Semancik S. 2009. Detecting chemical hazards with temperature-programmed microsensors: overcoming complex analytical problems with multidimensional databases? *Annu. Rev. Anal. Chem.* 2:463–84
47. Holloway AF, Nabok A, Thompson M, Ray AK, Wilkop T. 2004. Impedance analysis of the thickness shear mode resonator for organic vapour sensing. *Sens. Actuators B* 99:355–60
48. Josse F, Lukas R, Zhou R, Schneider S, Everhart D. 1996. AC-impedance-based chemical sensors for organic solvent vapors. *Sens. Actuators B* 35–36:363–69
49. Martin SJ, Frye GC. 1990. Surface acoustic wave response to changes in viscoelastic film properties. *Appl. Phys. Lett.* 57:1867–69
50. Wessendorf KO. 1993. The lever oscillator for use in high resistance resonator applications. In *Proc. 1993 Frequency Control Symp., New York*, pp. 711–17. Piscataway, NJ: IEEE
51. Hwang BJ, Yang JY, Lin CW. 2001. Recognition of alcohol vapor molecules by simultaneous measurements of resistance changes on polypyrrole-based composite thin films and mass changes on a piezoelectric crystal. *Sens. Actuators B* 75:67–75
52. Amrani MEH, Persaud KC, Payne PA. 1995. High-frequency measurements of conducting polymers: development of a new technique for sensing volatile chemicals. *Meas. Sci. Technol.* 6:1500–7
53. Yang RD, Fruhberger B, Park J, Kummel AC. 2006. Chemical identification using an impedance sensor based on dispersive charge transport. *Appl. Phys. Lett.* 88:074104
54. Rumyantsev S, Liu G, Shur MS, Potyraiolo RA, Balandin AA. 2012. Selective gas sensing with a single pristine graphene transistor. *Nano Lett.* 12:2294–98
55. Potyraiolo RA, Morris WG. 2007. Multianalyte chemical identification and quantitation using a single radio frequency identification sensor. *Anal. Chem.* 79:45–51
56. Potyraiolo RA, Mouquin H, Morris WG. 2008. Position-independent chemical quantitation with passive 13.56-MHz radio frequency identification (RFID) sensors. *Talanta* 75:624–28
57. Potyraiolo RA, Morris WG, Sivavec T, Tomlinson HW, Klensmeden S, Lindh K. 2009. RFID sensors based on ubiquitous passive 13.56-MHz RFID tags and complex impedance detection. *Wirel. Commun. Mob. Comput.* 9:1318–30
58. Potyraiolo RA, Surman C, Go S, Lee Y, Sivavec T, Morris WG. 2009. Development of radio-frequency identification sensors based on organic electronic sensing materials for selective detection of toxic vapors. *J. Appl. Phys.* 106:124902
59. Potyraiolo RA, Surman C, Morris WG, Go S, Lee Y, et al. 2010. Selective quantitation of vapors and their mixtures using individual passive multivariable RFID sensors. *IEEE Int. Conf. RFID, IEEE RFID, April 14–16, Orlando, FL*, pp. 22–28
60. Potyraiolo RA, Nagraj N, Surman C, Boudries H, Lai H, et al. 2012. Wireless sensors and sensor networks for homeland security applications. *Trends Anal. Chem.* 40:133–45
61. Potyraiolo RA, Morris WG. 2007. Wireless resonant sensor array for high-throughput screening of materials. *Rev. Sci. Instrum.* 78:072214
62. Potyraiolo RA, Boudries H, Naik RR. 2012. Multivariable MHz and GHz wireless chem/bio sensors for environmental, industrial, and security applications. In *Int. Meet. Chem. Sens. (IMCS), 14th, May 20–23, Nürnberg, Ger.*, pp. 399–402. Elsevier Sci.
63. Brahim S, Colbern S, Gump R, Grigorian L. 2008. Tailoring gas sensing properties of carbon nanotubes. *J. Appl. Phys.* 104:024502
64. Potyraiolo RA, Ding Z, Butts MD, Genovese SE, Deng T. 2008. Selective chemical sensing using structurally colored core-shell colloidal crystal films. *IEEE Sens. J.* 8:815–22
65. Potyraiolo RA, Ghiradella H, Vertiatchikh A, Dovidenko K, Cournoyer JR, Olson E. 2007. Morpho butterfly wing scales demonstrate highly selective vapour response. *Nat. Photonics* 1:123–28
66. Biró LP, Kertész K, Vértesy Z, Bálint Z. 2008. Photonic nanoarchitectures occurring in butterfly scales as selective gas/vapor sensors. *Proc. SPIE* 7057:705706
67. Gao Y, Xia Q, Liao G, Shi T. 2011. Sensitivity analysis of a bioinspired refractive index based gas sensor. *J. Bionic Eng.* 8:323–34
68. Eliason CM, Shawkey MD. 2010. Rapid, reversible response of iridescent feather color to ambient humidity. *Opt. Express* 18:21284–92

69. Kim JH, Moon JH, Lee S-Y, Park J. 2010. Biologically inspired humidity sensor based on three-dimensional photonic crystals. *Appl. Phys. Lett.* 97:103701
70. Kramer K, Hock B. 2004. Antibodies for biosensors. In *Ultrathin Electrochemical Chemo- and Biosensors*, ed. VM Mirsky, pp. 3–22. Berlin: Springer
71. Updike SJ, Hicks GP. 1967. The enzyme electrode. *Nature* 214:986–88
72. Jayasena SD. 1999. Aptamers: an emerging class of molecules that rival antibodies in diagnostics. *Clin. Chem.* 45:1628–50
73. Nanduri V, Sorokulova IB, Samoylov AM, Simonian AL, Petrenko VA, Vodyanov V. 2007. Phage as a molecular recognition element in biosensors immobilized by physical adsorption. *Biosens. Bioelectron.* 22:986–92
74. Lim JH, Park J, Ahn JH, Jin HJ, Hong S, Park TH. 2013. A peptide receptor-based bioelectronic nose for the real-time determination of seafood quality. *Biosens. Bioelectron.* 39:244–49
75. Mannoor MS, Zhang S, Link AJ, McAlpine MC. 2010. Electrical detection of pathogenic bacteria via immobilized antimicrobial peptides. *Proc. Natl. Acad. Sci. USA* 107:19207–12
76. Bousse L. 1996. Whole cell biosensors. *Sens. Actuators B* 34:270–75
77. Jin HJ, Lee SH, Kim TH, Park J, Song HS, et al. 2012. Nanovesicle-based bioelectronic nose platform mimicking human olfactory signal transduction. *Biosens. Bioelectron.* 35:335–41
78. Park SJ, Kwon OS, Lee SH, Song HS, Park TH, Jang J. 2012. Ultrasensitive flexible graphene based field-effect transistor (FET)-type bioelectronic nose. *Nano Lett.* 12:5082–90
79. Ko HJ, Park TH. 2008. Enhancement of odorant detection sensitivity by the expression of odorant-binding protein. *Biosens. Bioelectron.* 23:1017–23
80. Restrepo D, Miyamoto T, Bryant BP, Teeter JH. 1990. Odor stimuli trigger influx of calcium into olfactory neurons of the channel catfish. *Science* 249:1166–68
81. Horlacher T, Seeberger PH. 2008. Carbohydrate arrays as tools for research and diagnostics. *Chem. Soc. Rev.* 37:1414–22
82. Fukui S, Feizi T, Galustian C, Lawson AM, Chai W. 2002. Oligosaccharide microarrays for high-throughput detection and specificity assignments of carbohydrate-protein interactions. *Nat. Biotechnol.* 20:1011–17
83. Okahata Y, Shimizu O. 1987. Olfactory reception on a multilayer-coated piezoelectric crystal in a gas phase. *Langmuir* 3:1171–72
84. Mascini M, Macagnano A, Monti D, Del Carlo M, Paolesse R, et al. 2004. Piezoelectric sensors for dioxins: a biomimetic approach. *Biosens. Bioelectron.* 20:1203–10
85. Wu T-Z, Lo Y-R, Chan E-C. 2001. Exploring the recognized bio-mimicry materials for gas sensing. *Biosens. Bioelectron.* 16:945–53
86. Lu H-H, Rao YK, Wu T-Z, Tzeng Y-M. 2009. Direct characterization and quantification of volatile organic compounds by piezoelectric module chips sensor. *Sens. Actuators B* 137:741–46
87. White J, Truesdell K, Williams LB, AtKisson MS, Kauer JS. 2008. Solid-state, dye-labeled DNA detects volatile compounds in the vapor phase. *PLoS Biol.* 6:0030–36
88. Stubbs DD, Lee S-H, Hunt WD. 2002. Molecular recognition for electronic noses using surface acoustic wave immunoassay sensors. *IEEE Sens. J.* 2:294–300
89. Yano K, Yoshitake H, Bornscheuer UT, Schmid RD, Ikebukuro K, et al. 1997. Development of a chemical vapor sensor using piezoelectric quartz crystals with coated unusual lipids. *Anal. Chim. Acta* 340:41–48
90. Shafiqul Islam AKM, Ismail Z, Ahmad MN, Saad B, Othman AR, et al. 2005. Transient parameters of a coated quartz crystal microbalance sensor for the detection of volatile organic compounds (VOCs). *Sens. Actuators B* 109:238–43
91. Ichinohe S, Tanaka H, Kanno Y. 2007. Gas sensing by at-cut quartz crystal oscillator coated with mixed-lipid film. *Sens. Actuators B* 123:306–12
92. Wyszynski B, Somboon P, Nakamoto T. 2007. Pegylated lipids as coatings for QCM odor-sensors. *Sens. Actuators B* 121:538–44
93. Sugimoto I, Matsumoto T, Shimizu H, Munakata R, Seyama M, Takahashi J. 2009. The structures and gas-sorption properties of L-tyrosine films prepared by the Knudsen effusion method. *Thin Solid Films* 517:3817–23

94. Buck L, Axel R. 1991. A novel multigene family may encode odorant receptors: a molecular basis for odor recognition. *Cell* 65:175–87
95. Kobayashi S, Kitadai M, Sameshima K, Ishii Y, Tanaka A. 1999. A theoretical investigation of the conformation changing of dioxins in binding site of dioxin receptor model; role of absolute hardness–electronegativity diagrams for biological activity. *J. Mol. Struct.* 475:203–17
96. Sugimoto I, Nagaoka T, Seyama M, Nakamura M, Takahashi K. 2007. Classification and characterization of atmospheric VOCs based on sorption/desorption behaviors of plasma polymer films. *Sens. Actuators B* 124:53–61
97. Wyszynski B, Sekine M, Nakamoto T, Nakaso N, Noguchi K. 2010. Spherical SAW devices with self-assembled lipopolymers for odor-sensing. *Sens. Actuators B* 144:247–54
98. Hwang KS, Lee MH, Lee J, Yeo W-S, Lee JH, et al. 2011. Peptide receptor-based selective dinitrotoluene detection using a microcantilever sensor. *Biosens. Bioelectron.* 30:249–54
99. Zhao H, Ivic JM, Hashimoto M, Mikoshiba K, Firestein S. 1998. Functional expression of a mammalian odorant receptor. *Science* 279:237–42
100. Whaley SR, English DS, Hu EL, Barbara PF, Belcher AM. 2000. Selection of peptides with semiconductor binding specificity for directed nanocrystal assembly. *Nature* 405:665–68
101. Sarikaya M, Tamerler C, Jen AK-Y, Schulten K, Baneyx F. 2003. Molecular biomimetics: nanotechnology through biology. *Nat. Mater.* 2:577–85
102. Sanghvi AB, Miller KP-H, Belcher AM, Schmidt CE. 2005. Biomaterials functionalization using a novel peptide that selectively binds to a conducting polymer. *Nat. Mater.* 4:496–502
103. Jaworski JW, Raorane D, Huh JH, Majumdar A, Lee S-W. 2008. Evolutionary screening of biomimetic coatings for selective detection of explosives. *Langmuir* 24:4938–43
104. Koyama N, Kurihara K. 1972. Effect of odorants on lipid monolayers from bovine olfactory epithelium. *Nature* 236:402–4
105. Kasai N, Sugimoto I, Nakamura M, Katoh T. 1999. Odorant detection capability of QCR sensors coated with plasma deposited organic films. *Biosens. Bioelectron.* 14:533–39
106. Sugimoto I, Nakamura M, Kuwano H. 1994. Organic gas sorption characteristics of plasma-deposited amino acid films. *Anal. Chem.* 66:4316–23
107. Sugimoto I, Nakamura M, Kasai N, Katoh T. 2000. Gas-sorption effects on plasma polymer films characterized by XPS and quartz crystal resonator. *Polymer* 41:511–22
108. Kuang Z, Kim SN, Crookes-Goodson WJ, Farmer BL, Naik RR. 2010. Biomimetic chemosensor: designing peptide recognition elements for surface functionalization of carbon nanotube field effect transistors. *ACS Nano* 4:452–58
109. Staii C, Johnson AT Jr, Chen M, Gelperin A. 2005. DNA-decorated carbon nanotubes for chemical sensing. *Nano Lett.* 5:1774–78
110. Lu Y, Goldsmith BR, Kybert NJ, Johnson ATC. 2010. DNA-decorated graphene chemical sensors. *Appl. Phys. Lett.* 97:083107
111. Lee SH, Kwon OS, Song HS, Park SJ, Sung JH, et al. 2012. Mimicking the human smell sensing mechanism with an artificial nose platform. *Biomaterials* 33:1722–29
112. McAlpine MC, Agnew HD, Rohde RD, Blanco M, Ahmad H, et al. 2008. Peptide-nanowire hybrid materials for selective sensing of small molecules. *J. Am. Chem. Soc.* 130:9583–89
113. Nagraj N, Slocik JM, Phillips DM, Kelley-Loughnane N, Naik RR, Potyrailo RA. 2013. Selective sensing of vapors of similar dielectric constant using peptide-capped gold nanoparticles on individual multivariable transducers. *Analyst*. In press; doi: 10.1039/C3AN00088E
114. Mannoor MS, Tao H, Clayton JD, Sengupta A, Kaplan DL, et al. 2012. Graphene-based wireless bacteria detection on tooth enamel. *Nat. Commun.* 3:1767
115. Khamis SM, Jones RA, Johnson ATC, Preti G, Kwak J, Gelperin A. 2012. DNA-decorated carbon nanotube-based FETs as ultrasensitive chemical sensors: discrimination of homologues, structural isomers, and optical isomers. *AIP Adv.* 2:022110
116. Cui Y, Kim SN, Naik RR, McAlpine MC. 2012. Biomimetic peptide nanosensors. *Acc. Chem. Res.* 45:696–704
117. Goldsmith BR, Mitala JJ, Josue J, Castro A, Lerner MB, et al. 2011. Biomimetic chemical sensors using nanoelectronic readout of olfactory receptor proteins. *ACS Nano* 5:5408–16

118. Zuniga C, Rinaldi M, Khamis S, Jones T, Johnson A, Piazza G. 2009. Nanoenabled microelectro-mechanical sensor for volatile organic chemical detection. *Appl. Phys. Lett.* 94:223122
119. Wong SS, Joselevich E, Woolley AT, Cheung CL, Lieber CM. 1998. Covalently functionalized nanotubes as nanometresized probes in chemistry and biology. *Nature* 394:52–55
120. Chen RJ, Bangsaruntip S, Drouvalakis KA, Wong Shi Kam N, Shim M, et al. 2003. Noncovalent functionalization of carbon nanotubes for highly specific electronic biosensors. *Proc. Natl. Acad. Sci. USA* 100:4984–89
121. Johnson ATC, Khamis SM, Preti G, Kwak J, Gelperin A. 2010. DNA-coated nanosensors for breath analysis. *IEEE Sens. J.* 10:159–66
122. Johnson RR, Johnson CAT, Klein ML. 2010. The nature of DNA-base-carbon-nanotube interactions. *Small* 6:31–34
123. Pender MJ, Sowards LA, Hartgerink JD, Stone MO, Naik RR. 2006. Peptide-mediated formation of single-wall carbon nanotube composites. *Nano Lett.* 6:40–44
124. Wohltjen H, Snow AW. 1998. Colloidal metal-insulator-metal ensemble chemiresistor sensor. *Anal. Chem.* 70:2856–59
125. Mlsna TE, Cemalovic S, Warburton M, Hobson ST, Mlsna D, Patel SV. 2006. Chemicapacitive micro-sensors for chemical warfare agent and toxic industrial chemical detection. *Sens. Actuators B* 116: 192–201
126. Shawkey MD, D’Alba L, Wozny J, Eliason C, Koop JA, Jia L. 2011. Structural color change following hydration and dehydration of iridescent mourning dove (*Zenaidura macroura*) feathers. *Zoology* 114:59–68
127. Garrett NL, Vukusic P, Ogrin F, Sirotkin E, Winlove CP, Moger J. 2009. Spectroscopy on the wing: naturally inspired SERS substrates for biochemical analysis. *J. Biophoton.* 2:157–66
128. Yildirim A, Vural M, Yaman M, Bayindir M. 2011. Bioinspired optoelectronic nose with nanostructured wavelength-scalable hollow-core infrared fibers. *Adv. Mater.* 23:1263–67
129. Liu Z, Fan T, Zhang D, Gong X, Xu J. 2009. Hierarchically porous ZnO with high sensitivity and selectivity to H₂S derived from biotemplates. *Sens. Actuators B* 136:499–509
130. Song F, Su H, Han J, Lau WM, Moon W-J, Zhang D. 2012. Bioinspired hierarchical tin oxide scaffolds for enhanced gas sensing properties. *J. Phys. Chem. C* 116:10274–81
131. Michielsen K, Stavenga DG. 2008. Gyroid cuticular structures in butterfly wing scales: biological photonic crystals. *J. R. Soc. Interface* 5:85–94
132. Parker AR. 2000. 515 million years of structural colour. *J. Opt. A* 2:R15–28
133. Kinoshita S, Yoshioka S, Miyazaki J. 2008. Physics of structural colors. *Rep. Prog. Phys.* 71:076401
134. Vukusic P. 2005. Structural color effects in Lepidoptera. In *Structural Colors in Biological Systems. Principles and Applications*, ed. S Kinoshita, S Yoshioka, pp. 95–112. Osaka, Jpn.: Osaka Univ. Press
135. Doucet SM, Meadows MG. 2009. Iridescence: a functional perspective. *J. R. Soc. Interface* 6:S115–32
136. Seago AE, Brady P, Vigneron J-P, Schultz TD. 2009. Gold bugs and beyond: a review of iridescence and structural colour mechanisms in beetles (Coleoptera). *J. R. Soc. Interface* 6:S165–84
137. Rassart M, Colomer J-F, Tabarrant T, Vigneron JP. 2008. Diffractive hydrochromic effect in the cuticle of the hercules beetle *Dynastes hercules*. *New J. Phys.* 10:033014
138. Yang X, Peng Z, Zuo H, Shi T, Liao G. 2011. Using hierarchy architecture of *Morpho* butterfly scales for chemical sensing: experiment and modeling. *Sens. Actuators A* 167:367–73
139. Xia Y, Gates B, Yin Y, Lu Y. 2000. Monodispersed colloidal spheres: old materials with new applications. *Adv. Mater.* 12:693–713
140. Arsenault AC, Kitaev V, Manners I, Ozin GA, Mihi A, Míguez H. 2005. Vapor swellable colloidal photonic crystals with pressure tunability. *J. Mater. Chem.* 15:133–38
141. Yang H, Jiang P, Jiang B. 2012. Vapor detection enabled by self-assembled colloidal photonic crystals. *J. Colloid Interface Sci.* 370:11–18
142. Raymond KP, Burgess IB, Kinney MH, Lončar M, Aizenberg J. 2012. Combinatorial wetting in colour: an optofluidic nose. *Lab Chip* 12:3666–69
143. Zhang J-T, Wang L, Lamont DN, Velankar SS, Asher SA. 2012. Fabrication of large-area two-dimensional colloidal crystals. *Angew. Chem. Int. Ed.* 51:6117–20
144. Finkenzeller K. 2003. *RFID Handbook. Fundamentals and Applications in Contactless Smart Cards and Identification*. Hoboken, NJ: Wiley

145. Vullers RJM, van Schaijk R, Doms I, Van Hoof C, Mertens R. 2009. Micropower energy harvesting. *Solid State Electron.* 53:684–93
146. Gungor VC, Hancke GP. 2009. Industrial wireless sensor networks: challenges, design principles, and technical approaches. *IEEE Trans. Indust. Electron.* 56:4258–65
147. Becher C, Kaul P, Mitrovics J, Warmer J. 2010. The detection of evaporating hazardous material released from moving sources using a gas sensor network. *Sens. Actuators B* 146:513–20
148. Chen L, Yang S, Xi Y. 2010. Based on ZigBee wireless sensor network the monitoring system design for chemical production process toxic and harmful gas. *Int. Conf. Comput. Mechatron. Control Electron. Eng.* 4:425–28
149. Strelcov E, Dmitriev S, Button B, Cothren J, Sysoev V, Kolmakov A. 2008. Evidence of the self-heating effect on surface reactivity and gas sensing of metal oxide nanowire chemiresistors. *Nanotechnology* 19:355502
150. Pantelopoulos A, Bourbakis NG. 2010. A survey on wearable sensor-based systems for health monitoring and prognosis. *IEEE Trans. Syst. Man Cybern. C* 40:1–12
151. Diamond D, Coyle S, Scarmagnani S, Hayes J. 2008. Wireless sensor networks and chemo-/biosensing. *Chem. Rev.* 108:652–79
152. De Vito S, Di Palma P, Ambrosino C, Massera E, Burrasca G, et al. 2011. Wireless sensor networks for distributed chemical sensing: addressing power consumption limits with on-board intelligence. *IEEE Sens. J.* 11:947–55
153. Link JR, Sailor MJ. 2003. Smart dust: self-assembling, self-orienting photonic crystals of porous Si. *Proc. Natl. Acad. Sci. USA* 100:10607–10
154. Vyas R, Lakafofis V, Lee H, Shaker G, Yang L, et al. 2011. Inkjet printed, self powered, wireless sensors for environmental, gas, and authentication-based sensing. *IEEE Sens. J.* 11:3139–52
155. Potyrailo RA, Burns A, Surman C, Lee DJ, McGinniss E. 2012. Multivariable passive RFID vapor sensors: roll-to-roll fabrication on a flexible substrate. *Analyst* 137:2777–81
156. Kim D-H, Lu N, Ma R, Kim Y-S, Kim R-H, et al. 2011. Epidermal electronics. *Science* 333:838–43
157. Jung M, Kim J, Noh J, Lim N, Lim C, et al. 2010. All-printed and roll-to-roll-printable 13.56-mHz-operated 1-bit RF tag on plastic foils. *IEEE Trans. Electron Dev.* 57:571–80
158. Tao H, Brenckle MA, Yang M, Zhang J, Liu M, et al. 2012. Silk-based conformal, adhesive, edible food sensors. *Adv. Mater.* 24:1067–72
159. Potyrailo RA, Nagraj N, Tang Z, Mondello FJ, Surman C, Morris W. 2012. Battery-free radio frequency identification (RFID) sensors for food quality and safety. *J. Agric. Food Chem.* 60:8535–43
160. Potyrailo RA, Morris WG. 2011. *Methods and systems for calibration of RFID sensors.* US Patent No. 7,911,345
161. Preechaburana P, Gonzalez MC, Suska A, Filippini D. 2012. Surface plasmon resonance chemical sensing on cell phones. *Angew. Chem. Int. Ed.* 51:11585–88



Contents

Computational Materials (Richard LeSar & Simon Phillpot, Keynote Topic Editors)

Computational Approaches for the Dynamics of Structure Formation in Self-Assembling Polymeric Materials <i>Marcus Müller and Juan J. de Pablo</i>	1
Density Functional Theory Models for Radiation Damage <i>S.L. Dudarev</i>	35
Electronic-Structure Theory of Organic Semiconductors: Charge-Transport Parameters and Metal/Organic Interfaces <i>Veaceslav Coropceanu, Hong Li, Paul Winget, Lingyun Zhu, and Jean-Luc Brédas</i>	63
Phase-Field Model for Microstructure Evolution at the Mesoscopic Scale <i>Ingo Steinbach</i>	89
Reactive Potentials for Advanced Atomistic Simulations <i>Tao Liang, Yun Kyung Shin, Yu-Ting Cheng, Dundar E. Yilmaz, Karthik Guda Vishnu, Osvalds Verners, Chenyu Zou, Simon R. Phillpot, Susan B. Sinnott, and Adri C.T. van Duin</i>	109
Simulating Mechanical Behavior of Ceramics Under Extreme Conditions <i>I. Szlufarska, K.T. Ramesh, and D.H. Warner</i>	131
Uncertainty Quantification in Multiscale Simulation of Materials: A Prospective <i>Aleksandr Chernatynskiy, Simon R. Phillpot, and Richard LeSar</i>	157

Modern Optical Microscopy Techniques in Materials Research (Venkatraman Gopalan, Keynote Topic Editor)

Nanoscale Hard X-Ray Microscopy Methods for Materials Studies <i>Martin Holt, Ross Harder, Robert Winarski, and Volker Rose</i>	183
Nonlinear Optical Microscopy of Single Nanostructures <i>Libai Huang and Ji-Xin Cheng</i>	213

Real-Time, Subwavelength Terahertz Imaging <i>F. Blanchard, A. Doi, T. Tanaka, and K. Tanaka</i>	237
Superresolution Multidimensional Imaging with Structured Illumination Microscopy <i>Aurélie Jost and Rainer Heintzmann</i>	261
Vesicle Photonics <i>A.E. Vasdekis, E.A. Scott, S. Roke, J.A. Hubbell, and D. Psaltis</i>	283
Current Interest	
Bionanomaterials and Bioinspired Nanostructures for Selective Vapor Sensing <i>Radislav Potyrailo and Rajesh R. Naik</i>	307
Electroplating Using Ionic Liquids <i>Andrew P. Abbott, Gero Frisch, and Karl S. Ryder</i>	335
Engineering Crystal Morphology <i>Preshit Dandekar, Zubin B. Kuvadia, and Michael F. Doberty</i>	359
Flexoelectric Effect in Solids <i>Pavlo Zubko, Gustau Catalan, and Alexander K. Tagantsev</i>	387
Mesoscale Domains and Nature of the Relaxor State by Piezoresponse Force Microscopy <i>V.V. Shvartsman, B. Dkhil, and A.L. Kholkin</i>	423
Nanowire Heterostructures <i>Jerome K. Hyun, Shixiong Zhang, and Lincoln J. Laubon</i>	451
Phosphors for Solid-State White Lighting <i>Nathan C. George, Kristin A. Denault, and Ram Seshadri</i>	481
Polymer Electrolytes <i>Daniel T. Hallinan Jr. and Nitash P. Balsara</i>	503
Templated Chemically Deposited Semiconductor Optical Fiber Materials <i>Justin R. Sparks, Pier J.A. Sazio, Venkatraman Gopalan, and John V. Badding</i>	527
Water Vapor–Mediated Volatilization of High-Temperature Materials <i>Peter J. Meschter, Elizabeth J. Opila, and Nathan S. Jacobson</i>	559
The Yin-Yang of Rigidity Sensing: How Forces and Mechanical Properties Regulate the Cellular Response to Materials <i>Ingmar Schoen, Beth L. Pruitt, and Viola Vogel</i>	589